ANNUAL REVIEWS

Annual Review of Physical Chemistry

Mapping Structural Dynamics of Proteins with Femtosecond Stimulated Raman Spectroscopy

Chong Fang and Longteng Tang

Department of Chemistry, Oregon State University, Corvallis, Oregon 97331, USA; email: Chong.Fang@oregonstate.edu

Annu. Rev. Phys. Chem. 2020. 71:239–65

First published as a Review in Advance on February 19, 2020

The *Annual Review of Physical Chemistry* is online at physchem.annualreviews.org

https://doi.org/10.1146/annurev-physchem-071119-040154

Keywords

protein structural dynamics, ultrafast Raman spectroscopy, photochemical reaction coordinates, vibrational coupling, resonance enhancement, excited-state relaxation

Abstract

The structure–function relationships of biomolecules have captured the interest and imagination of the scientific community and general public since the field of structural biology emerged to enable the molecular understanding of life processes. Proteins that play numerous functional roles in cellular processes have remained in the forefront of research, inspiring new characterization techniques. In this review, we present key theoretical concepts and recent experimental strategies using femtosecond stimulated Raman spectroscopy (FSRS) to map the structural dynamics of proteins, highlighting the flexible chromophores on ultrafast timescales. In particular, wavelength-tunable FSRS exploits dynamic resonance conditions to track transient-species-dependent vibrational motions, enabling rational design to alter functions. Various ways of capturing excited-state chromophore structural snapshots in the time and/or frequency domains are discussed. Continuous development of experimental methodologies, synergistic correlation with theoretical modeling, and the expansion to other nonequilibrium, photoswitchable, and controllable protein systems will greatly advance the chemical, physical, and biological sciences.

1. INTRODUCTION

Femtosecond stimulated Raman spectroscopy (FSRS): recent development has focused on the tunability of ultrafast laser pulses to achieve desirable resonance conditions

Franck-Condon (FC) region: vertical excitation into the FC region is due to displaced potential energy surfaces from the electronic ground to excited state

Proteins are a diverse group of fascinating biomolecules that play a myriad of roles in life processes. Besides characterization of their functions in vivo, a fundamental understanding of how proteins operate in their native environments demands a rigorous physical chemistry approach. Structural motions responsible for intramolecular and intermolecular interactions on a wide range of timescales, from femtoseconds to seconds and beyond, serve as the foundation for protein functions. The commonly used techniques of X-ray crystallography and nuclear magnetic resonance (NMR) spectroscopy have been prolific in solving protein structures to build sophisticated models for their functions, but a visualization of protein motions (particularly at the active site) in real time is highly desirable and can be achieved by structural dynamics techniques with simultaneously high spatial and temporal resolutions. Such work is highly transformative and of substantial current interest in chemistry, biophysics and photobiology, bioengineering, and life sciences (1–4), which constitutes the background and motivation for this review.

This article starts by summarizing eight key considerations for implementing ultrafast molecular spectroscopy to study proteins in situ. First, a noninvasive approach ensures that protein samples remain largely intact before and after spectroscopic measurements. Second, spectral information provides comprehensive and deep insights into protein functions with a direct link to timescales and/or conformations. Third, physiological environments for in vitro protein characterization typically require the omnipresent water as solvent. Fourth, photosensitive proteins can be model systems to map nonequilibrium structural dynamics, while reversible or irreversible light-induced changes need to be tracked. Fifth, vibrational spectroscopy in the electronic ground state (S_0) can capture protein motions at thermal equilibrium (5). Transient vibrational spectra in the electronic excited state can be collected after a well-defined time zero of photoexcitation to track nonequilibrium protein motions. Sixth, site-specific information reveals the microscopic structural dynamics underlying macroscopic protein functions. Seventh, while most pump–probe techniques monitor vibronic couplings from correlated electronic and nuclear motions (5–8), elucidating the anharmonic coupling matrix directly in the vibrational domain is desirable. Eighth, when accessing functional roles of vibrational motions, an ensemble measurement captures structural snapshots averaged over a sufficiently large sample pool instead of stochastic fluctuations (9).

Due to these considerations, recent developments of femtosecond stimulated Raman spectroscopy (FSRS) have provided previously unavailable structural dynamics information for proteins (2, 10–28). FSRS has also been used to investigate various materials, from charge-transfer complexes to conjugated materials (29–33), that are outside the scope of this review. Following earlier reviews about FSRS (9, 12, 34), we present salient aspects of the FSRS technique in tracking structural motions at equilibrium (e.g., in S_0) and nonequilibrium conditions (e.g., in electronic excited states), also highlighting new experiments that expand FSRS into the anti-Stokes region (15, 23, 35, 36) and enhance the tunability of laser pulses to exploit dynamic resonance Raman conditions (35, 37–42). From the ultraviolet (UV) to near-infrared (NIR) region, representative photoinduced processes include excited-state proton transfer (ESPT) in fluorescent proteins (FPs) and FP-based biosensors, *cis-trans* isomerization, and energy transfer inside proteins.

Because of the high sensitivity of FSRS probing vibrational dynamics after photoexcitation, this methodology provides an appealing platform to examine and improve theoretical calculations for nuclear motions in real time, as fast as coherent proton movement out of the Franck-Condon (FC) region (43–45). Such ab initio quantum chemical calculations with sufficient accuracy and predictive power will be instrumental in improving our fundamental understanding of chemical reactivity on molecular timescales and in systematically elucidating rational design principles. Accumulation and analysis of FSRS data on proteins (9, 14, 34) will substantiate and advance current

efforts toward biophysical and biochemical characterization with testable hypotheses. Subsequent engineering endeavors will help to achieve the desirable protein functions in physiologically relevant environments.

Free induction decay (FID): the decoherence of vibrational motions as a consequence of solvent collision and other energy dissipation pathways

2. BACKGROUND AND EMERGING CONCEPTS IN FSRS

2.1. Overview of FSRS Methodology

FSRS is currently being developed into a versatile and general methodology to film atomic motions that power chemistry (2, 9, 10, 13–16, 22–24, 34–38, 46–49). FSRS can be performed as a two-pulse (i.e., Raman pump and probe) or three-pulse (i.e., Raman pump and probe with a preceding actinic pump) technique. Stimulated Raman uses ultrafast laser pulses to provide the means to compare vibrational spectra as a function of pH, temperature, pressure, or added reagent (34, 50, 51). Furthermore, simultaneously high resolution in time and spectral domains enables FSRS to collect the nonequilibrium vibrational signatures of photosensitive molecules.

Figure 1*a* presents a schematic of an optical FSRS setup with three incident laser pulses (i.e., actinic pump, Raman pump, and Raman probe) in a noncollinear geometry that focus onto the sample (typically inside a solution cell). There is a phase-locked optical chopper in the Raman pump beam path and a shutter in the actinic pump beam path. The transmitted Raman probe carrying the stimulated Raman signal is allowed to travel further and enter a spectrograph before imaging onto a CCD (charge-coupled device) array camera. This femtosecond-picosecond-femtosecond pulse sequence in FSRS makes it possible to observe molecular structural dynamics starting from the FC region after femtosecond actinic photoexcitation. The absence of competing light–matter interaction pathways due to the picosecond Raman pump keeps the vibrational coherences relatively straightforward during nonlinear signal generation (see Section 2.3), which benefits data analysis and interpretation in situations where the biomolecular electronic resonance conditions are dynamic and complex, while protein samples are generally fragile and have a low radiation-damage threshold (2, 14, 16, 34, 52).

2.2. Phase Matching and Energy Ladder Diagrams at Resonance Conditions

The FSRS spectrum is customarily collected in a noncollinear geometry with a small crossing angle between the coincident Raman pump and probe pulses, as well as a photoexcitation pulse (**Figure 1*a***) if the photoinduced processes are of interest (14, 47, 53). The nonlinear four-wave mixing involves two interactions of the molecular system with the picosecond Raman pump and one interaction with the femtosecond Raman probe. The entire process can be regarded as six-wave mixing if two earlier interactions between the molecular Hamiltonian and actinic pump are counted in generating the excited-state population as well as initial vibrational coherences, which are not to be confused with the probing vibrational coherences depicted as free induction decay (FID) in **Figure 2** (9, 54, 55).

Because the wave vectors associated with two Raman pump interactions cancel each other, the FSRS signal is emitted via self-phase matching in the probe direction only (12, 47, 56). Although the signal is heterodyne detected by the collinear Raman probe and therefore not background free (5, 52, 57, 58), the synchronization of the CCD camera with a 1-kHz or higher repetition rate of the laser amplifier system enables the effective use of each laser pulse to significantly increase the signal-to-noise ratio (SNR) during FSRS data collection. Taking the ratio of the Raman probe intensity profile with and without the Raman pump yields the stimulated Raman gain, offset by –1, assuming that the gain is typically small (47).

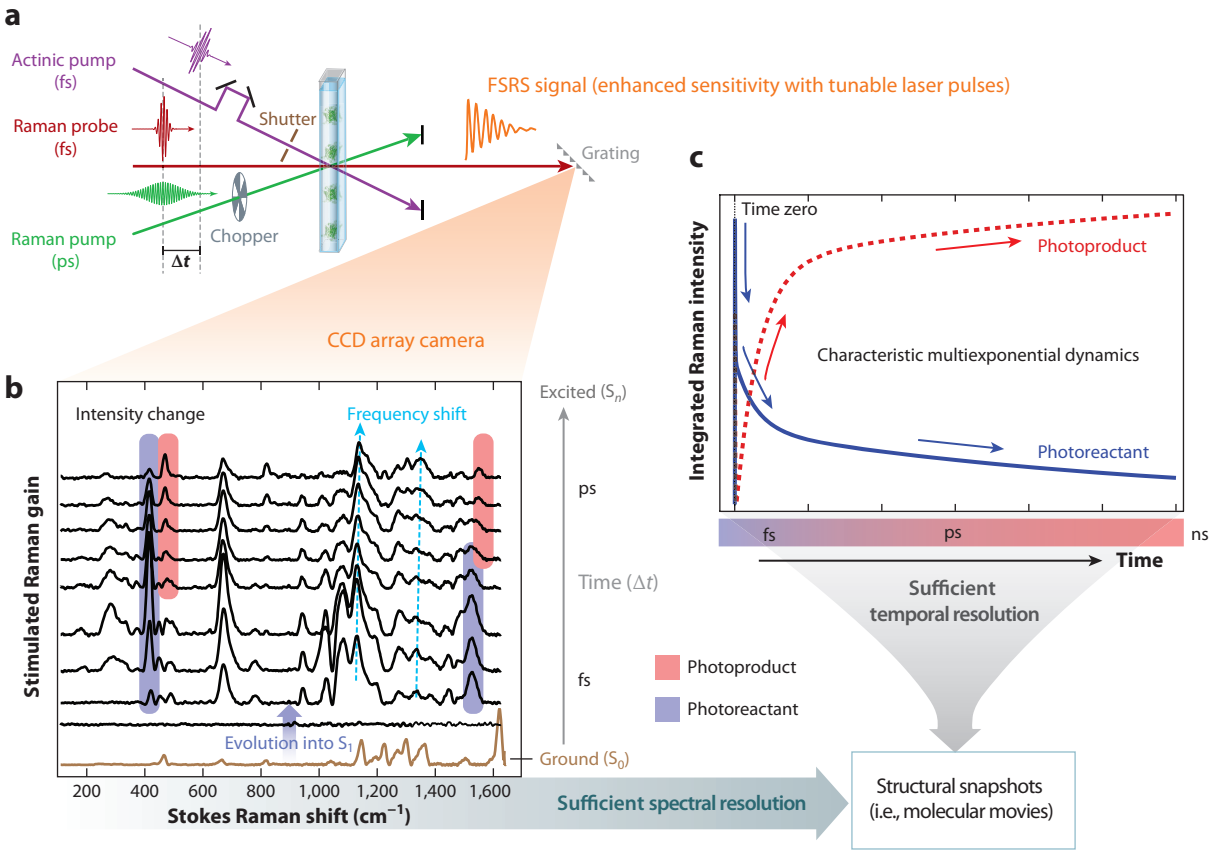

Figure 1

Time-resolved FSRS reveals molecular structural evolution. (*a*) The FSRS experiment employs a sequence of femtosecond-picosecond-femtosecond laser pulses in the ultraviolet to near-infrared region to study proteins in solution with the spatially dispersed detection of transient spectral signals. (*b*) Representative time-stacked plot on ultrafast timescales exhibits initial vibrational mode evolution from the electronic ground (S_0, *brown*) to excited states (S_n, e.g., S_1, *black*). Colored bars (photoreactant, *purple*; photoproduct, *red*) highlight several marker bands. (*c*) Raman mode-dependent intensity (or frequency) dynamics in the excited state map the photoreactant decay (*blue*) and photoproduct rise (*red*), typically exhibiting multiexponential behavior with characteristic time constants (here depicted by *arrows*). Sufficient temporal and spectral resolutions enable the capture of structural snapshots, i.e., molecular movies. Abbreviations: CCD, charge-coupled device; FSRS, femtosecond stimulated Raman spectroscopy.

In FSRS, the Raman-active modes in condensed media are monitored as a function of the time delay between photoexcitation and stimulated Raman process, therefore highlighting the importance of using femtosecond actinic-pump and Raman-probe pulses. The picosecond Raman pump is crucial for FSRS because it ensures that the signal can be collected in the frequency domain—it is not necessary to time resolve the FID of vibrational coherences generated by the simultaneous arrival of the Raman pump and probe (**Figure 2*a*,*b***). The spectral resolution is high because the Raman pump does not significantly truncate the FID, especially those vibrations in the electronic excited state that rapidly dephase (12, 14, 34, 56). The observed peak frequency is not instantaneous but is rather a time-averaged frequency convoluted with the Raman pump duration and FID, which results in a reduced magnitude of the frequency change (2, 54). Moreover, a much higher peak density versus a continuous-wave light source makes stimulated Raman spectroscopy

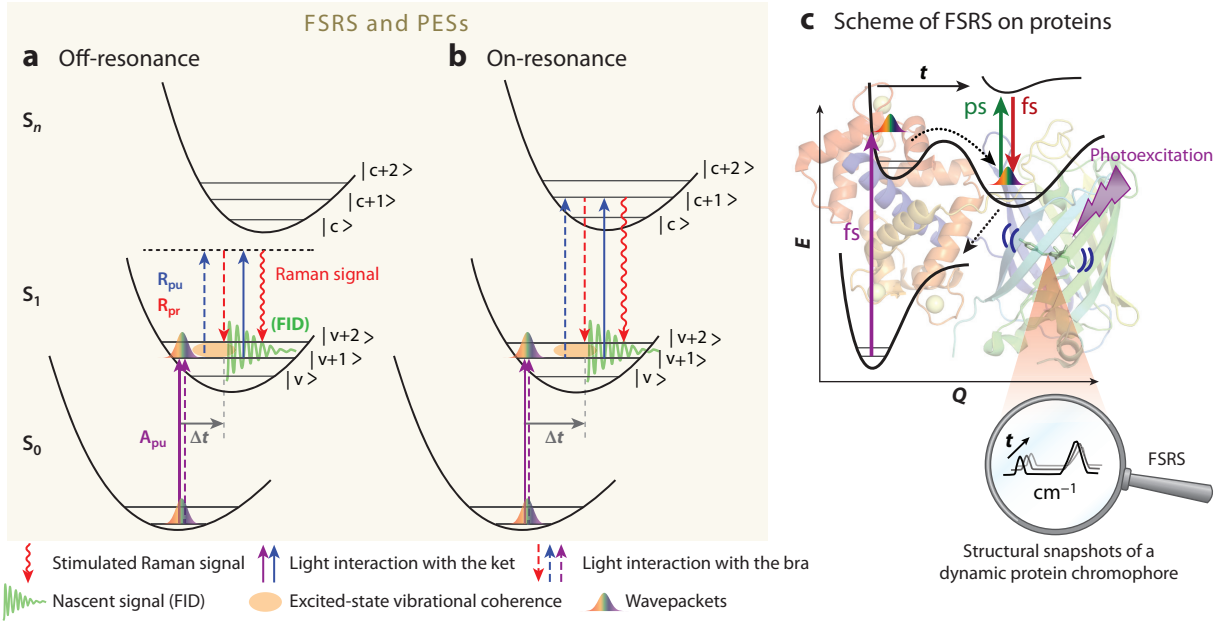

Figure 2

Schematic of the light–matter interaction and signal generation in an excited-state FSRS experiment at (*a*) off-resonance and (*b*) on-resonance conditions. The PESs are shown from the electronic ground state (S_0) to higher electronic states (S_1, S_n), with vibrational levels drawn as horizontal bars (quantum numbers are listed in kets). After the actinic pump (A_{pu}, *purple*) that populates S_1, the excited-state vibrational coherence being probed is highlighted by the orange ellipse, and the nascent signal (*green damping oscillation*) undergoes FID while continuing to interact with the picosecond Raman pump (R_{pu}, *blue*). The femtosecond Raman probe (R_{pr}, *red*) is necessary to generate the vibrational coherence by interacting with the system only once. The stimulated Raman signal (*red wavy arrow*) is emitted in the phase-matched direction collinear with R_{pr}. The solid and dashed vertical arrows represent light interaction with the ket and bra side of a molecular density matrix, respectively. Excited-state absorption is shown for the electronic resonance achieved in panel *b*, which could be stimulated emission in other cases. (*c*) Illustration of a time-resolved FSRS study of proteins capturing structural snapshots of a dynamic chromophore (wiggles by *blue curves*) navigating the excited-state PES (plotted with energy, *E*, as the ordinate and nuclear coordinate, *Q*, as the abscissa) in the protein pocket. Dotted arrows depict the internal conversion between electronic states. Abbreviations: FID, free induction decay; FSRS, femtosecond stimulated Raman spectroscopy; PES, potential energy surface. Panels *a* and *b* adapted from Reference 55 with permission; copyright 2019 AIP Publishing.

much more efficient than spontaneous Raman, and electronic resonance conditions can also be exploited to enhance the SNR. Recent efforts in generating a tunable picosecond Raman pump across the UV to NIR region (37, 48, 59) have been reviewed in detail by Dietze & Mathies (34). In tandem, the tunable Raman probe is derived from the supercontinuum white light (SCWL) generated in a thin medium such as sapphire, calcium fluoride, or deionized water (42, 47, 53, 60). Alternatively, the background-free Raman probe from a broadband upconverted multicolor array (BUMA) (37, 57, 59, 61–63) based on cascaded four-wave mixing in an ultrathin condensed-phase medium can provide further tunability into the near-UV (e.g., 340–470 nm) (59, 61, 62) or NIR region (e.g., 660–780 nm) (37, 57, 63).

Typical features in time-resolved FSRS data (**Figure 1*b***) highlight the convenience and power of tracking individual Raman modes while the nonstationary wave packets launched by the femtosecond actinic pump navigate the excited-state potential energy surface (PES) (**Figure 2*c***). Consequently, the kinetic intensity plot (**Figure 1*c***) of various Raman marker bands manifests the photoreactant decay and photoproduct rise in one graph, providing crucial and self-corroborating

Potential energy surface (PES): crucial in describing electronic wavefunctions and the associated nuclear motions

mechanistic information of the photoinduced multidimensional reaction coordinate with chemical bond precision and femtosecond time resolution.

2.3. Multiple Vibrational Coherences Generated and Evolving in FSRS

FSRS performed in the mixed time-frequency domain results in an effective separation between the impulsively excited coherent motions (64) and the stimulated Raman signal (46, 47, 56). The interplay between these vibrational coherences enables unique FSRS inquiry into the anharmonic coupling matrix in a mode-dependent manner across a broad spectral range (2, 9, 14).

Low-frequency modes are generally considered crucial during photochemical reactions (2, 6, 8, 10, 31, 38, 53, 65, 66), which could orchestrate photoproduct formation, energy dissipation, and conformational dynamics. These modes act as an effective internal sink for the excess excitation energy commonly involved in ultrafast spectroscopy to probe light–matter interactions. Upon electronic excitation, these collective motions commonly display strong vibronic coupling to the upward transition and hence large Huang-Rhys factors and FC activities (2, 21, 26). Subsequent energy flow out of these initially excited modes into other modes depends on vibrational coupling in the electronic excited state (while the wave-packet counterpart in S_0 is harmonic) (67, 68), which provides a clear platform for FSRS to track such molecular cooperativity in action through the Raman peak intensity or frequency quantum beating as a function of time (9, 38, 69).

Though not definitive, spectral oscillations observed in FSRS are closely related to functional motions. First, the ensemble-average nature of the experiment ensures that stochastic fluctuations and random molecular orientations in the laboratory frame are averaged out. Second, coherent skeletal motions are impulsively driven by the femtosecond actinic pump, and for a typical ~35-fs Fourier-transform-limited pulse centered at ~800 nm, low-frequency modes up to ~500 cm^{-1} can be activated (9, 38, 53, 70). Third, the gating or tuning modes are commonly retrieved from notable oscillations of other vibrational modes that can be strongly modulated via the vibrational coupling matrix (2, 9, 16, 38). The fact that a few characteristic marker bands stand out implies that they project strongly onto the reaction coordinates, while others dissipate energy and fade away. This rationale affords level ground to evaluate vibrational coupling, intramolecular (31) as well as intermolecular in nature (38), and to pursue a mechanistic understanding of intrinsic energy relaxation and chemical reactivity particularly in the electronic excited states.

2.4. Dynamic Resonance Raman Enhancement in Tunable FSRS

In FSRS, fluorescence rejection (12, 14, 34, 47) is an important attribute that works with resonance Raman enhancement to observe vibrational modes. This capability is achieved spatially by collecting the self-phase-matched signal along the probe beam path, and temporally by collecting the stimulated Raman peaks from time zero to hundreds of picoseconds. It is important to consider two experimental scenarios in relation to this property of FSRS. When the Raman pump–probe pair locates to the red side (14, 47, 53) or blue side (36, 40, 41) of the spontaneous emission band, the detection window does not cover the emission range so the fluorescence background is automatically absent. When the Raman pump–probe pair spectrally overlaps with the spontaneous emission band, the Raman gain calculation ensures that the fluorescence background appears in both the numerator and denominator and hence does not contribute to the ratio (assuming that the Raman pump does not significantly affect the fluorescence profile) (17, 35, 38). Notably, the exploitation of a stimulated emission (SE) band to enhance transient vibrational features highlights the unique power of FSRS to achieve fluorescence suppression even under this circumstance. The picosecond Raman pump can be optimized in excited-state FSRS to take advantage

of the preresonance effect in reference to an SE band, but without too much power to induce notable depletion of the excited-state population (34, 35). In this way, structural dynamics at the chemical bond level (i.e., atomic choreography governing chemical reactivity) can be dissected.

Using pyranine as a model photoacid in methanol, which inhibits proton transfer, we reported dynamic Raman line shapes with a tunable Raman pump from 625 to 510 nm (36). A systematic investigation of FSRS signal line shapes from gain to dispersive to loss as the Raman pump is tuned across an evolving excited-state absorption (ESA) band, as well as a comparative study of the Stokes versus anti-Stokes peak intensity and frequency dynamics with the same Raman pump, reveals the interplay between the molecular dynamics (i.e., electronic and nuclear motions) and FSRS pulse sequence (**Figures 1** and **2**). Notably, the Raman pump plays less of a role in the observed Raman line shape, but it does affect the broad spectral baseline that largely mimics the transient absorption (TA) spectral profile (9, 34–36, 38, 71). The proximity of the Raman probe to a transient electronic peak maximum (e.g., ESA) or minimum (e.g., SE) may play a more critical role in generating dispersive features. Therefore, a general rule for FSRS experimentation is to keep the Raman pump and probe encompassed on the far-red side of the electronic feature (but not completely off-resonant) so nondispersive line shapes can be observed with sufficient SNR (72).

2.5. Experimental Implementation of FSRS and Comparison to Infrared Studies of Proteins

Following linear spectroscopy such as UV-visible measurement on any given sample, the experimental procedure typically involves performing femtosecond transient absorption (fs-TA) before FSRS to select an optimal combination of actinic pump, Raman pump, and Raman probe wavelengths (31, 38, 39). The wavelength tunability for this particular sequence of femtosecond, picosecond, and femtosecond pulses is crucial to exploit the resonance Raman effect and to enhance the vibrational features of transient molecular species, which hold the key to unlocking the multidimensional reaction coordinates leading to macroscopic functionality. In principle, the impulsive broadband Raman approach can record transient Raman modes in the excited state by Fourier transform analysis of the time-domain interference signal (26, 65, 73), and the ultrabroad bandwidth of the sub-10-fs laser pulse can help to map the entire anharmonic coupling matrix from the low- to high-frequency vibrational modes of interest. However, following the initial actinic pump, the fs-TA approach using two femtosecond pulses in the electronic excited state could potentially access different information when compared to the FSRS approach in the mixed time-frequency domain, particularly when different wavelengths are used for the picosecond and femtosecond laser pulses to achieve various electronic resonance conditions after the femtosecond photoexcitation pulse. Caution is thus required when comparing the spectroscopic results from these different approaches because various experimental parameters could be readily involved in generating the signal (see Section 3.1.1).

Some appealing attributes of FSRS for studying protein structural dynamics are brought to light by comparison with the powerful two-dimensional infrared (2D-IR) spectroscopy, which can capture an almost instantaneous snapshot of protein structural distributions at equilibrium, as presented in the seminal work of Hochstrasser, Hamm, Lim, and colleagues (5, 74–79) and recently reviewed by Zanni and coworkers (4). The FSRS method tracks photoinduced processes in nonequilibrium states using an actinic pump without the need for isotope labeling (75) because the chromophore itself affords site specificity. FSRS can exploit resonance Raman enhancement to selectively probe vibrational features from reactant through intermediate to product, therefore exposing multiple vibrations simultaneously to delineate the reaction coordinate. No line shape or phase factor adjustment is required to process the experimental spectra because the time-resolved

FSRS data are directly collected in the frequency domain (14, 34, 48, 49, 52). A typical FSRS spectrum spans from approximately 200 cm^{-1} to 2,200 cm^{-1}, mainly depending upon the bandwidth of the femtosecond Raman probe that stimulates Raman scattering photons in reference to the picosecond Raman pump. A 2D-FSRS coherence map can then be generated after removing the multiexponential decay component and Fourier transforming the residual coherent components at individual Raman peaks across the spectral window (9, 31). Alternatively, Moran and coworkers (58) have used diffractive optics and demonstrated four- and five-beam implementations of resonance FSRS with background-free signal collection on heme proteins. In their description of these experiments, they discussed the typical dominance of the direct fifth-order response over the unwanted third-order cascades for dilute solute samples in solution (versus pure liquids or concentrated mixtures in which the cascades could dominate and complicate the apparent anharmonic coupling scheme) (80, 81). Current understanding is that resonant excitation and 2D-FSRS in the excited state of solute molecules lead to an effective way to reveal vibrational anharmonicities between the low-frequency wave packets and high-frequency reporter modes, with the former motions impulsively excited by the actinic pump in FSRS.

In regard to this, one can say that 2D-IR exhibits characteristic line shapes with homogeneous and inhomogeneous contributions, providing insights into spectral diffusion processes in the ground state or as a function of external perturbation (5). In addition, time-resolved IR (TRIR) spectroscopy with an actinic pump can monitor the photoexcited chromophore and surrounding residues in proteins (82), which often leads to highly overlapped spectra from the ground- and excited-state IR-absorption signals. FSRS, however, specializes in tracking vibrational motions of protein active sites with intrinsic sensitivity to light-sensitive components such as an embedded chromophore. In particular, simultaneous observation of vibrational modes spanning a broad spectral range (e.g., from low-frequency delocalized modes <200 cm^{-1} to high-frequency localized modes $>2{,}000$ cm^{-1}) of the photoexcited molecular systems in aqueous buffer solution, with various electronic resonance conditions to selectively enhance the characteristic Raman modes associated with transient species during a photoinduced reaction, comprises the major advantage of FSRS to experimentally investigate the structural dynamics of proteins.

3. ELUCIDATING STRUCTURAL DYNAMICS OF PROTEINS BY FSRS

Multitudinous functions of proteins originate from their underlying chemical reactions. Typical reactions in biological systems include proton transfer, electron transfer, isomerization, and energy relaxation, which are all related to protein structural motions. For example, proton transfer can be viewed as stretching a hydrogen bond until dissociation occurs (38, 83). Meanwhile, pertinent vibrational motions are highly coupled with electron flow (52, 53). The isomerization process is often facilitated by a bond-twisting motion (10, 20, 65, 84–86), and vibrational relaxation represents one of the most effective pathways to dissipate energy (27, 35, 78, 87, 88).

Elucidating the structure–function relationships of proteins has motivated the science and engineering community for decades. With an expanding repertoire of protein structures from techniques such as X-ray crystallography, NMR, and cryogenic electron microscopy in the Protein Data Bank (PDB), research into the structural dynamics of proteins on native timescales has gained further momentum owing to the advancement of ultrafast laser technologies. The main reason to exploit emergent tunable FSRS technology (see Section 2) to study proteins is rooted in the multidimensional PES, leading to various resonance conditions to enhance Raman modes with functional relevance.

In this section, we review the applications of FSRS to the study of proteins that involve various photophysical and photochemical processes, aiming to highlight the breadth and depth of

investigations into previously unexplored or underexplored areas regarding protein structural dynamics under equilibrium and nonequilibrium conditions. Both cases could be highly relevant for protein functions, while the latter case also involves the protein response to an external stimulus (e.g., temperature, pressure, pH, ions or other reagents, or light, which is the focus here). Moreover, the role of dynamic conformational ensembles has attracted great interest not only due to the structural heterogeneity revealed by these state-of-the-art techniques (5, 25, 34) but also by protein potential energy landscape simulations (89). The famous quote "everything that living things do can be understood in terms of the jiggling and wiggling of atoms" by Richard Feynman (90) in 1963 remains highly relevant to this day. The quest to map chemical reactivities and biological functions at the molecular level (2, 6–8, 10, 16, 21, 26, 74, 76–79, 84, 91–95) has continued to inspire technical advances and innovative experiments across disciplines from physical chemistry and chemical physics, spectroscopy and optics, and chemical and structural biology, to protein engineering.

3.1. Tracking the Excited-State Proton Transfer Reaction Inside Fluorescent Proteins and Fluorescent Protein–Based Biosensors

A common critique of ultrafast spectroscopy is the difficulty of convincingly correlating the observed ultrafast electronic and/or nuclear motions to the functionality of the system under study. For example, the fastest protein folding events occur on a microsecond timescale (96), and it is challenging to establish the causal relationship between the femtosecond-to-picosecond motions and microsecond processes or other protein functional events on longer timescales (4, 78, 79). In contrast, the main function of FPs is emitting fluorescence on the nanosecond timescale, an ultrafast process in its own merit. Therefore, electronic and structural motions on the femtosecond-to-picosecond timescale directly precede fluorescence without a notable gap and are responsible for the characteristic radiative emission (82, 83, 97, 98). Besides the critical importance of understanding biological functions from the bottom up, such microscopic insights into how FPs and biosensors work on molecular timescales have profound implications for rational design and practical applications in bioimaging, bioengineering, and biomedicine.

3.1.1. Revealing functional skeletal motions of SYG chromophore in fluorescent proteins.

The discovery of green fluorescent protein (GFP) from the Pacific Northwest jellyfish *Aequorea victoria* (99) as a genetically encodable fluorescent biomarker has revolutionized molecular and cellular biology (97, 100, 101). Because GFP tolerates a variety of structural manipulations, it allowed protein engineers to convert FPs into FP-based biosensors. Extensive X-ray crystallography and biophysical and biochemical studies on GFP and mutants (91, 92, 102, 103) have reached consensus that ESPT is the putative reaction pathway for the neutral chromophore. However, the working mechanism of wild-type (wt) GFP—wtGFP—leading to its bright green fluorescence [quantum yield (QY) = 0.8] remained elusive until the first FSRS study by Fang, Mathies, and coworkers (2). In that work, excited-state Raman marker bands of the Ser65-Tyr66-Gly67 (SYG) neutral chromophore in the electronic excited state (A^* form) exhibited a biexponential decay with a concomitant rise of the intermediate deprotonated chromophore (I^* form) on the picosecond timescale. The C=O and C=N stretching modes at opposite ends of the conjugated chromophore display out-of-phase intensity and frequency oscillations with a period of ~280 fs, corresponding to an impulsively excited coherent motion at ~120 cm^{-1} (**Figure 3*a***). This key motion helps optimize the chromophore phase space for ESPT, although such a functional role does not require the wagging motion to persist throughout ESPT because the net evolution along such a coordinate in the first picosecond could shift the electron density and nuclear positions in the direction of

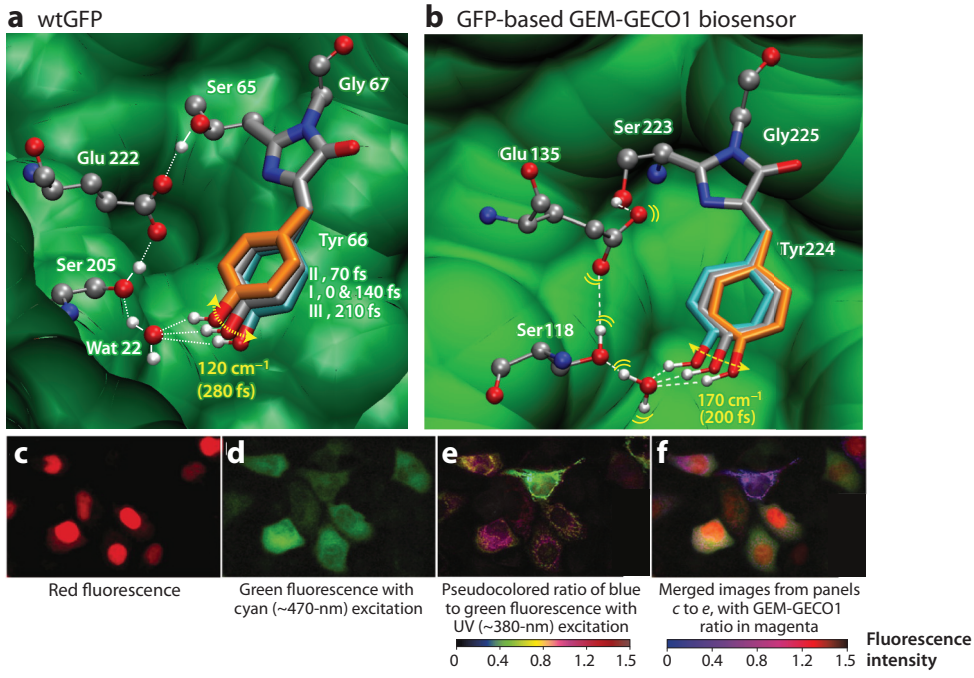

Figure 3

Dominant low-frequency skeletal motions inside fluorescent proteins elucidated by excited-state femtosecond stimulated Raman spectroscopy. (*a*) The 120-cm^{-1} phenolic ring out-of-plane wagging gates excited-state proton transfer in wtGFP with a conserved water molecule [Wat22 in crystal structure, Protein Data Bank (PDB) ID 1EMB] (92) above and to one side of the chromophore plane. Panel *a* reproduced from Reference 2 with permission; copyright 2009 Nature Publishing Group. (*b*) The 170-cm^{-1} phenolic ring in-plane rocking facilitates excited-state proton transfer inside the GFP domain of the Ca^{2+}-free GEM-GECO1 biosensor, involving a labile water molecule and a largely in-plane Ser118 derived from equilibrium molecular dynamics simulations [initial geometric constraints from the Ca^{2+}-free GCaMP2 crystal structure, PDB ID 3EKJ (106), with all the GEM-GECO1 specific mutations and a sufficient surrounding water shell]. Panel *b* reproduced from Reference 16 with permission; copyright 2014 National Academy of Sciences. (*c–f*) Multicolor imaging with GECOs that expand the color palette for Ca^{2+} indicators in vivo. Panels *c–e* show HeLa cells transfected with the nucleus-localized R-GECO1, cytoplasmic G-GECO1, and mitochondria-localized GEM-GECO1 protein biosensors. Panel *f* shows merged images from panels *c* to *e* with the GEM-GECO1 pseudocolored ratio in magenta. Panels *c–f* adapted from Reference 104 with permission; copyright 2011 American Association for the Advancement of Science. Abbreviations: GECO, genetically encoded calcium ion indicator for optical imaging; GFP, green fluorescent protein; wt, wild type.

tautomerism (2). This study firmly established FSRS as a powerful structural dynamics technique to answer the open questions about FPs: What motions are fundamentally responsible for colorful emissions on molecular timescales, and what are rational design principles to change fluorescence properties?

The essence of this 2D-FSRS approach (31, 38, 69) (see Section 2.5) lies in the recording of the ultrafast evolution of multiple vibrational modes across a wide spectral window. Fourier transform analysis of the coherent spectral oscillations retrieves underlying modulation modes. In an ideal experimental case (e.g., accessing the low-frequency region in excited-state FSRS), those active skeletal motions can be directly observed for a photoacidic chromophore in solution (e.g., ~180 and 280 cm^{-1}) (38) or inside the GFP pocket (e.g., ~460 and 505 cm^{-1}) (18).

Fujisawa et al. (22) used femtosecond time-resolved impulsive stimulated Raman spectroscopy (TR-ISRS) (see Section 2.5) to revisit coherence-mediated ESPT in wtGFP; they observed the actinic-pump-induced A* coherence modulating the emerging SE band of I* with a similar skeletal mode at ~105 cm^{-1}. This mode matches the ~120-cm^{-1} mode of wtGFP in aqueous buffer solution from time-resolved FSRS within experimental error (2). Anharmonic vibrational coupling between this mode and a high-frequency A* phenolic C–H bending mode at ~1,142 cm^{-1} was also observed. However, the growth of an I* phenolate CO stretching mode at ~1,295 cm^{-1} displayed very small modulation, suggesting that low-frequency coherent motion may not play a dominant role in ESPT at room temperature (22). Critically, the TR-ISRS result could be due to a different stimulated Raman pump–probe resonance condition in S_1 (sub–7 fs, 520–700 nm) versus time-resolved FSRS using a 794-nm Raman pump (~3 ps) and an SCWL probe (~20 fs, 840–960 nm) (2). The picosecond Raman pump provides an energy reservoir to create an averaged image of transient vibrational coherence FID in S_1 (**Figure 2**), placing most emphasis on the initial instantaneous frequency. The altered peak intensity ratios involving high-frequency modes in TR-ISRS could arise from the collection scheme of the time-domain interference signal, which requires the phase-stable scanning of two sub-7-fs pulses over a relatively long time to achieve sufficient SNR at each time delay (22, 73). Such an extended detection time could pose experimental challenges, including the protein photostability and damage threshold. We expect a more informative comparison with similar resonance conditions (for all the laser pulses) and SNR in the spectral regions of interest (particularly for the high-frequency modes) between stimulated Raman signals collected using different versions of the FSRS setup.

Dynamic resonance enhancement: a unique attribute of wavelength-tunable FSRS in achieving vibrational-mode-specific resonance Raman enhancement as the molecular system evolves in a nonequilibrium state

To corroborate the functional role of low-frequency modes, we studied a Ca^{2+} biosensor called GEM-GECO1 (16). The series of biosensors included green/blue dual emission, improved green, red intensiometric, and excitation ratiometric genetically encoded Ca^{2+} indicators for optical imaging, named GECOs (**Figure 3*b–f***) (104). They belong to the GCaMP family of Ca^{2+} biosensors with three major subunits: the Ca^{2+}-sensing calmodulin (CaM), its binding client M13 peptide, and the circularly permuted (cp)GFP (105, 106). The CaM subunit undergoes large-scale structural changes and wraps around M13 in the presence of Ca^{2+}. These changes, especially at the interfacial region close to the β-barrel opening where CaM interacts with cpGFP, alter the chromophore environment and modulate the fluorescence of the Ca^{2+}-bound biosensor.

To facilitate discussions with a common theme, we present **Figure 4**, which summarizes the chromophore structures and main spectral results from various FP-based biosensors. In the FSRS study of GEM-GECO1 (16), the modes above ~800 cm^{-1} were monitored from S_0 to S_1 toward the fluorescent state, although the modes below 300 cm^{-1} were challenging to observe due to the scattering from protein solution as well as the 800-nm residual in SCWL (18). Based on the Raman mode intensity plot (see **Figure 4*a*** for the 1,180-cm^{-1} mode, the phenol ring-H and bridge C–H rocking of the chromophore), the Ca^{2+}-free biosensor undergoes ESPT with an ~27-ps time constant. In contrast, this reaction is inhibited in the Ca^{2+}-bound biosensor with a much longer time constant of ~590 ps, attributed to nonradiative relaxation pathways from the A* state (16).

These results showed that resonance enhancement of the A* Raman features before and during ESPT is ubiquitous for GFP systems, and an 800-nm Raman pump in Stokes FSRS is effective for recording the excited-state conformational dynamics (2, 16, 18). After ESPT, the I* state has both ESA and SE bands shifted to ~500–600 nm (17, 22, 91, 103), a largely conserved electronic feature for the SYG and threonine-tyrosine-glycine (TYG) chromophore found in enhanced GFP (92) or superfolder GFP (107). Theoretical consideration for dynamic resonance enhancement (see Section 2.4) thus suggests the use of an ~530-nm Raman pump to track I* dynamics on the receiving end (17, 19, 24, 27) in correlation with the 800-nm Raman pump results focusing on A* dynamics on the giving end (see Section 3.1.2) (16, 18).

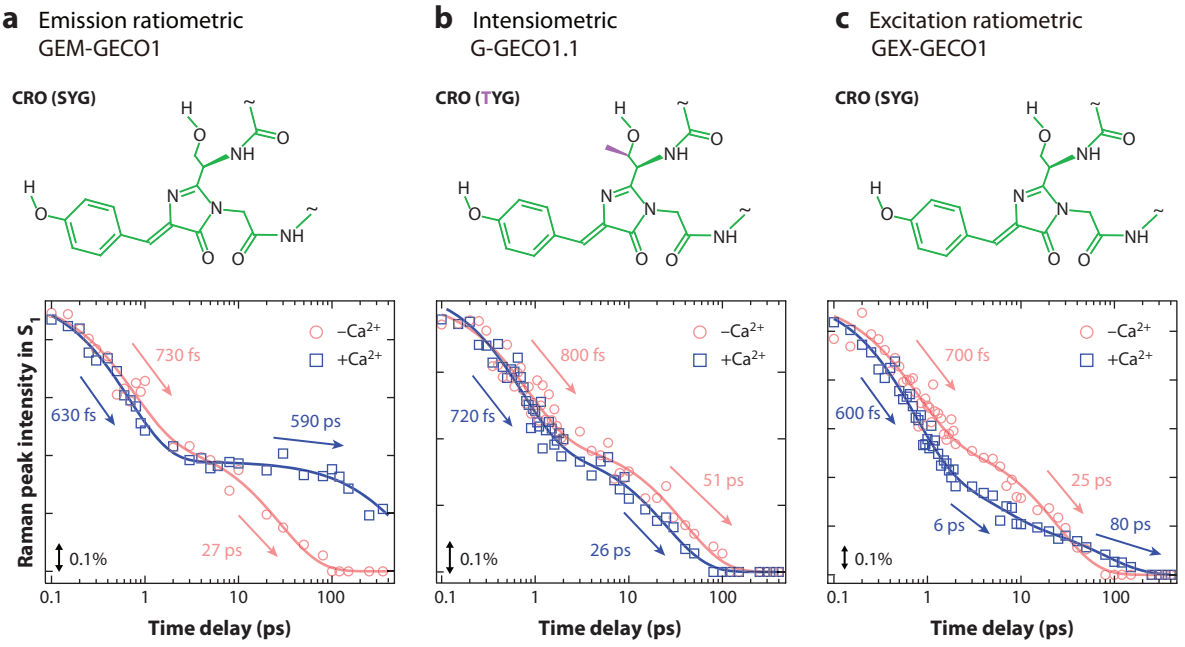

Figure 4

Comparative Raman intensity decay of the neutral chromophore (CRO) inside fluorescent protein biosensors following 400-nm photoexcitation. (*a–c*) The SYG/TYG/SYG chromophore in GEM-GECO1/G-GECO1.1/GEX-GECO1 calcium biosensors. The ~1,180-cm^{-1} mode intensity dynamics of the Ca^{2+}-free (*red circles*) and -bound (*blue squares*) biosensors exhibit clear differences with various protein functions (*top row*). The least-squares fits are shown in solid curves with associated time constants (beside their corresponding *color-coded arrows*) in the semilogarithmic plots. The stimulated Raman gain magnitude of 0.1% is depicted in each bottom panel. Panel *a* adapted from Reference 16 with permission; copyright 2014 National Academy of Sciences. Panel *b* adapted from Reference 17 with permission; copyright 2015 John Wiley and Sons. Panel *c* adapted from Reference 25 with permission; copyright 2017 American Chemical Society. Abbreviations: GECO, genetically encoded calcium ion indicator for optical imaging; SYG, Ser65-Tyr66-Gly67; TYG, threonine-tyrosine-glycine.

Importantly, a different ~170-cm^{-1} mode was revealed to modulate several vibrational marker bands in S_1 of the Ca^{2+}-free GEM-GECO1 biosensor (16). Chromophore structural constraints from molecular dynamics simulations (**Figure 3*b***) were used for density functional theory calculations (108), leading to a phenolic ring rocking motion at this vibrational frequency. In stark contrast, a much more irregular oscillation pattern was observed in the Ca^{2+}-bound biosensor, indicating multiple modulation modes in an altered chromophore environment as the hydrophobic Pro377 of CaM domain moves closer to the interfacial region after Ca^{2+} binding.

The experimentally uncovered distinct variation of a dominant low-frequency motion after photoexcitation substantiates its functional role in gating the ESPT reaction by modulating the H-bonding configuration between chromophore phenolic hydroxyl, intervening water molecules, and an adjacent serine (acting as the first protein residue to transfer the proton away). If such a low-frequency mode is merely a spectator mode, it makes little sense for the altered environment to feature another spectator mode instead of showing both for the identical chromophore. This is particularly true as the GFP interior becomes more hydrophilic and flexible in GEM-GECO1 due to the β-barrel opening toward the interfacial region with CaM (104). Also, the impulsive excitation of low-frequency modes is not necessary in nature, possibly after incoherent light irradiation (such as sunlight), but those skeletal motions still exist and couple to certain high-frequency modes

as governed by the molecular Hamiltonian. Nonlinear coherent spectroscopy such as FSRS generates multiple vibrational coherences with a sophisticated pulse sequence (**Figures 1*a*** and **2**), so we can synchronize and amplify the otherwise unsynchronized and undetectable oscillatory signals. In this vein, the mismatch between the FID time of the impulsively excited low-frequency vibrational coherences and the ESPT time constant is a consequence of experimental setup and detection scheme, which cannot be directly used to refute the functional relevance of those robust low-frequency motions or vibronic coherence features, particularly regarding the state mixing and directional energy flow in biomolecules (2, 9, 16, 68, 86, 93, 109).

A subsequent FSRS study (25) of a green excitation ratiometric FP biosensor called GEX-GECO1 with an SYG chromophore, which reaches the Ca^{2+}-binding equilibrium the fastest among all GECOs, showed two- versus three-exponential decay of the A* marker band in the Ca^{2+}-free and -bound biosensors (**Figure 4*c***), respectively. To corroborate spectral results in the absence of X-ray crystal structures, we performed 10-ns equilibrium molecular dynamics simulations, which highlighted one dominant interoxygen distance in the Ca^{2+}-free biosensor (∼6.0 Å) and a bimodal distribution of interoxygen distances in the Ca^{2+}-bound biosensor (∼5.0 and 6.5 Å). These results provide crucial structural constraints to substantiate the ESPT time constants of ∼25 ps and ∼6 ps, 80 ps in the Ca^{2+}-free and -bound states, respectively, revealing the previously hidden structural inhomogeneity inside the protein pocket (25). The analogous interoxygen distance in wtGFP is ∼4.3 Å (PDB ID 1EMB as in **Figure 3*a***) with an associated ∼5-ps ESPT time constant (2, 92).

At this point, a unified picture has emerged about structural dynamics information obtained by FSRS on FPs and FP biosensors. Differences in time constants, structural inhomogeneity, and emission properties (see **Figure 4*a*** versus **Figure 4*c*** for the same SYG chromophore) (16, 25) all emphasize that the chromophore structure cannot be the sole determinant for protein function. Instead, what lies at the heart of structure–function relationships is the interplay between the chromophore structure and protein environment. Furthermore, recent experimental and theoretical work has suggested that protein electrostatics may be more important than steric effects in enhancing fluorescence upon light irradiation of the embedded chromophore (25, 110, 111).

3.1.2. Dissecting structural dynamics of TYG chromophore in fluorescent proteins. Notably, the TYG chromophore represents an excellent system, with just an extra methyl group at the imidazolinone end compared to the SYG chromophore. In the green intensiometric FP biosensor G-GECO1.1, the neutral and anionic chromophore absorbs at ∼400 and ∼500 nm, respectively (17). Several excited-state Raman modes exhibit a sub-200-fs frequency shift reminiscent of the small-scale proton motions inside GEM-GECO1 (18), revealing the conserved nature for chromophore wiggling motions during initial energy dissipation on the subpicosecond timescale. After the coherently launched wave packets move out of the FC region, ESPT is faster in the Ca^{2+}-bound state (∼26 ps) than in the Ca^{2+}-free state (∼51 ps) by fitting the A* marker band intensity decay (**Figure 4*b***).

To confirm the occurrence of ESPT, Fang and coworkers (17, 19, 37) used tunable FSRS with an ∼530-nm Raman pump to track I* formation with resonance enhancement by an SE band. The ∼1,370-cm^{-1} mode (chromophore phenol ring-H rocking, CO stretching, and bridge C–H rocking in I*) rises with ∼22- and 42-ps time constants in the Ca^{2+}-bound and -free biosensors, respectively, matching the A* mode decay. This work represents the first time that tunable FSRS (see Section 2.5) was employed to track photoproduct formation after an ESPT reaction inside proteins (17).

In close relation to the structural dynamics insights into FP biosensors, tunable FSRS has recently demonstrated its resolving power in the engineered GFP-S205V single mutant (28)

and GFP-S65T/S205V double mutant (112). The absence of a complexed CaM domain allows a focused study of ESPT mechanisms inside a well-protected β-barrel. In GFP-S205V, three Raman pump wavelengths of 800, 539, and 504 nm were used to reveal an ESPT time constant of ~300 ps, a competing vibrational cooling time constant of ~190 ps for the trapped A* species, and an approximately 1,330-cm^{-1} I* mode with bridge-H motions displaying prominent dispersive line shapes (see Section 2.4) in the anti-Stokes FSRS with a 504-nm Raman pump (28). In GFP-S65T/S205V, separate tracking of the A* and I* spectral features using an 800- and 550-nm Raman pump, respectively, elucidates a previously hidden ~4-ps component that precedes the large-scale proton dissociation along the PT wire on an approximately 110-ps timescale (112). These findings led to a stepwise-concerted-hybrid reaction mechanism that could be a general strategy for proteins evolved in nature to avoid high-energy intermediates and efficiently perform their biological functions.

3.1.3. FSRS informs rational design of protein biosensors. Systematic tunable FSRS studies of FP biosensors have elucidated the ESPT mechanisms and functional low-frequency modes prior to fluorescence. In 2017, Fang and coworkers (24) reported the first tuning of GEM-GECO1 with a single-site mutation, Pro377Arg (P377R), which converted the green-blue emission ratiometric biosensor into a green excitation ratiometric biosensor (**Figure 5**). Larger structural inhomogeneity was found inside the Ca^{2+}-bound state, revealing effective trapping of multiple subpopulations in the neutral SYG chromophore by the mutated arginine (27). The ESPT time constants of ~16 and 90 ps are longer than those (~6 and 80 ps) inside GEX-GECO1 (25), indicating that structural heterogeneity is common in proteins, and key mutations based on ultrafast spectroscopic insights can guide protein engineering.

Direct comparison between GEM-GECO1 and its P377R mutant with altered emission lends additional support to the functional role of low-frequency motions (see Section 3.1.1). Such modulating modes are retrieved by discrete Fourier transform of oscillations in the Raman-mode intensity or frequency plot (31, 38, 53). The conserved ~180-cm^{-1} mode in the Ca^{2+}-free state (**Figure 5*a–c***) confirms the dominance of this phenolic ring rocking on the femtosecond-to-picosecond timescale to facilitate ESPT when the chromophore senses the β-barrel opening while residue 377 is distant. Upon Ca^{2+} binding (**Figure 5*d–f***), the photoexcited chromophore wiggles more in the first few picoseconds, displaying more low-frequency modes from phenolic ring rocking to wagging (16, 24). The vibrational coupling matrix is in accord with the structural inhomogeneity of the Ca^{2+}-bound biosensor chromophore pocket as more energy dissipation pathways become available with the nearby Arg377 modifying steric effects and electrostatics. Tuning the interplay between chromophore photoacidity and protein environment can thus help select a specific low-frequency motion to enhance ESPT with a constrained chromophore and tight H-bonding network (25, 27, 52). The fluorescence modulation properties of FP biosensors could then be rationally improved.

3.2. Elucidating Chromophore Twisting Motions Inside Proteins

Despite holding paramount importance for FPs, ESPT is just one of the ubiquitous reactions that occur in proteins. FSRS has also enabled tracking of ultrafast isomerization in proteins. In fact, some of the earliest FSRS reports focused on the photoinduced 11-*cis* to all-*trans* isomerization of retinal in rhodopsin (10) and the all-*trans* to 13-*cis* reaction in bacteriorhodopsin (11). Past reviews summarized FSRS results on rhodopsin (9, 12, 14, 34) with recent experiments using an alternative FSRS approach (113), but a few salient points merit discussion here. The retinal isomerization proceeds through a conical intersection (CI) within 50 fs and the photorhodopsin

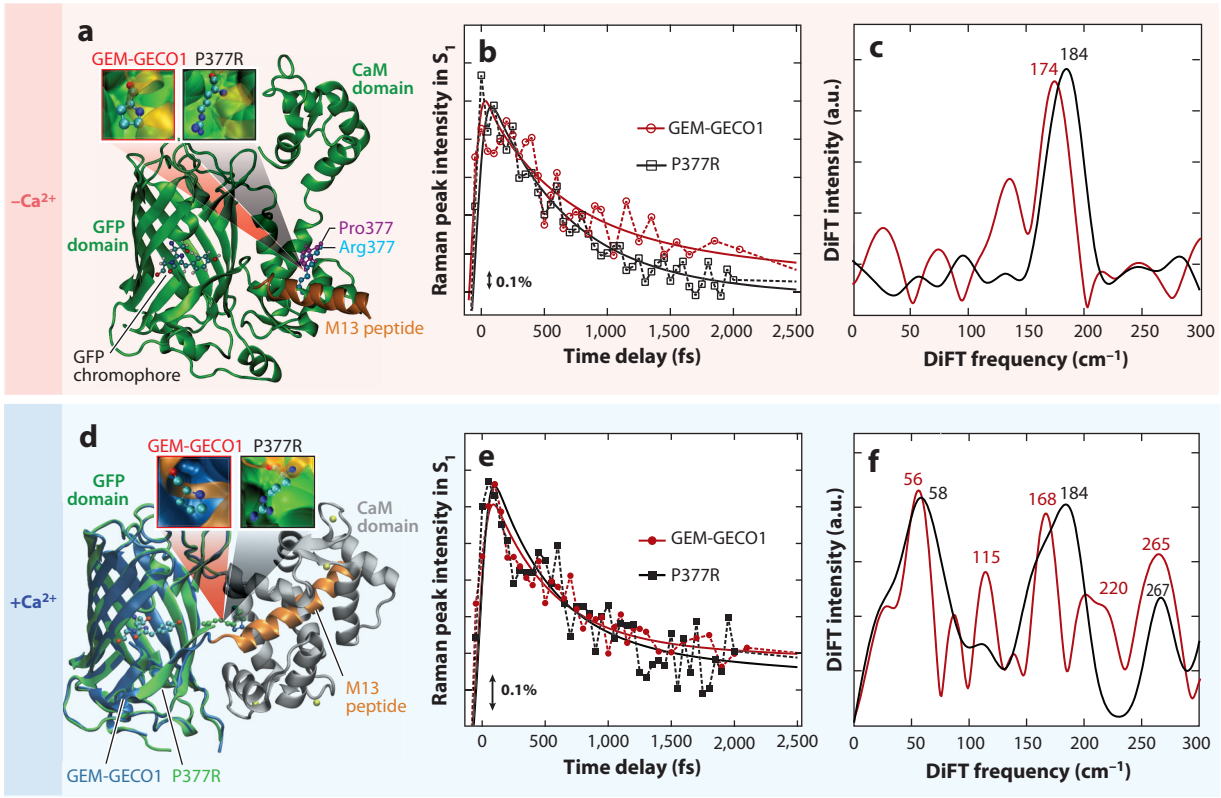

Figure 5

Tuning fluorescent protein–based Ca^{2+} biosensors with a single-site mutation. (*a*) Overlaid structures of the Ca^{2+}-free GEM-GECO1 and its P377R mutant. Pro377 (*magenta*) and Arg377 (*cyan*) in GEM-GECO1 (*red box*) and P377R (*black box*) are enlarged in their local environments, respectively. Different domains and the chromophore of the biosensor are labeled. (*b*) Coherent oscillations in the ~1,575-cm^{-1} mode intensity in S_1 of the Ca^{2+}-free GEM-GECO1 (*red*) and P377R (*black*). Least-squares fits to the incoherent components are shown by the solid curves. (*c*) DiFT of coherent oscillations in panel *b* yielding an approximately 180-cm^{-1} mode. (*d*) Structures of the Ca^{2+}-bound GEM-GECO1 biosensor (based on the GCaMP2 structure, PDB ID 3EVR) (105) and its P377R mutant. Pro377 (*blue*) and Arg377 (*green*) in GEM-GECO1 and P377R are enlarged (inside *colored boxes*), respectively. Four Ca^{2+} ions bound to CaM are shown as yellow spheres. (*e*) Coherent oscillations in the 1,575-cm^{-1} mode of the Ca^{2+}-bound GEM-GECO1 (*red*) and P377R (*black*). (*f*) DiFT of coherent oscillations in panel *e* yielding multiple competing low-frequency modes. Figure adapted from Reference 24 with permission; copyright 2017 PCCP Owner Societies. Abbreviations: CaM, calmodulin; DiFT, discrete Fourier transform; GECO, genetically encoded calcium ion indicator for optical imaging; GFP, green fluorescent protein; M13, chicken myosin light chain kinase; PDB, Protein Data Bank.

intermediate is produced on the ground state in ~140 fs (66, 84). Structural motions were extracted from FSRS data: An anharmonic coupling between a hydrogen out-of-plane motion and a double-bond torsion was uncovered in the excited state. Mode coupling was described as promoting vibrationally coherent passage through a CI into the photoproduct ground state (10, 66). New studies by Kukura and colleagues (20, 113) using time-domain impulsive Raman spectroscopy, however, have shown that vibrational coherence through a CI is more nuanced than originally thought. The issue is further complicated by recent failures to implement quantum coherent control in the rhodopsin, bacteriorhodopsin, and isorhodopsin systems at ambient conditions (114), as well as a recent 2D photon echo spectroscopic study that suggests that key vibronic transitions initiate the vibrationally coherent photochemistry of vision by going through a CI on an ~30-fs

timescale (8). Another recent report explored the vibrational phase-dependent isotope effect by TA experiments and nonadiabatic trajectory quantum mechanics/molecular mechanics simulations (94), showing that deuteration of the isomerizing H_{11}–C_{11} = C_{12}–H_{12} double bond of the 11-*cis* retinal chromophore in rhodopsin leads to unexpected, marked changes in the photoisomerization QY.

Many other photoreceptor proteins exhibit light-induced chromophore twisting that can be studied by FSRS. Because phytochromes use the covalently bound bilin chromophores to enable photoconversion between different light-absorbing forms (13), they can be categorized as photoswitchable proteins. Photoswitching and photoconversion capabilities also exist in the GFP family, which hold great promise for super-resolution imaging (115–118). Generally speaking, the chromophore *cis-trans* isomerization is the common mechanism of reversible photoswitching, while other contributing factors include the protonation states, chromophore planarity, and electrostatic interactions and steric hindrance within a protein pocket. For example, reversible photoswitching in the GFP-like Dronpa has been studied by X-ray crystallography (119), solution NMR at ambient temperatures (120), fs-TA spectroscopy (121), and TRIR (122), which correlated the *cis-trans* isomerization of the Cys62-Tyr63-Gly64 (CYG) chromophore with an intricate rearrangement of nearby protein residues and revealed that the first step of dark-to-bright photoconversion may involve ESPT on the picosecond timescale. Recently, the photoconvertible FP Kaede with a His62-Tyr63-Gly64 (HYG) chromophore was studied by time-resolved fluorescence and TA spectroscopy (123), and another photoconvertible Kaede-like FP LEA (least-evolved ancestor) with the same HYG chromophore was investigated by time-resolved UV-visible spectroscopy, ground-state FSRS, and TA spectroscopy (124). On the combined reversible and irreversible photoswitching front, the tetrameric IrisFP undergoes multiple photoinduced transformations (125, 126) that render an intriguing protein optical highlighter for time-resolved optical and X-ray spectroscopy, aiming to establish the ultrafast interplay between chromophore isomerization and protonation state (127).

Along this line of inquiry, we have started to investigate the photoswitchable mTFP0.7 (evolved from the nonphotoconvertible *Clavularia* CFP484) (116) using excited-state FSRS with various actinic-pump and Raman-pump wavelengths to track the fluorescent on and off states. Despite the rather small fraction of chromophores involved due to low photoswitching QY [e.g., $<1 \times 10^{-3}$ for the on-to-off transition and <0.5 for the off-to-on transition (128)], our data showed a number of preresonantly enhanced Raman bands from ~400–1,700 cm^{-1} tracking chromophore structural dynamics (mainly the *trans*-to-*cis* isomerization) up to 600 ps in the electronic excited state during the photoinduced off-to-on transition. Recently, ground-state resonance FSRS has been conducted in our lab on the green-to-red photoconvertible LEA-GFP (129) to unveil trapped species responsible for low photoconversion QY, which laid the groundwork (124) for excited-state FSRS of the HYG chromophore and its surroundings. The goal is to elucidate how ultrafast molecular events are coupled to the ensuing nonequilibrium transformations (52, 86) in LEA, which likely involve an irreversible sequence of chromophore twisting, chemical bond breaking and making to extend the π-conjugation, and generation of red fluorescence on much longer timescales.

3.3. Delineating Energy Transfer Pathways in Light-Harvesting and Heme Proteins

Regarding nonfluorescent proteins with diverse functions, vibrational coherences in four related tetrameric photosynthetic phycobiliproteins for light harvesting [i.e., from cryptophyte algae using the plant antenna complex or light-harvesting complex (LHC)] have been recorded by broadband fs-TA and ground-state FSRS (130). These species have similar properties from color to

size, and each protein consists of eight covalently bound chromophores with various geometric constraints and absorption profiles. The experiments were designed to disentangle overlapping spectral contributions by using TA coherent oscillations and FSRS peak frequencies to track the excited- and ground-state nuclear wave packet motions, respectively, hence providing new details about vibronic couplings and their potential functional roles for energy transfer. This work should motivate 2D-FSRS (see Sections 2.5 and 3.1.1) to elucidate vibronic and vibrational couplings during photoinduced reactions in proteins, especially after optimal wavelengths are determined for the photoexcitation pulse and stimulated Raman pulses (see Sections 2.3 and 2.4).

In 2018, the Kennis group (131) studied a photoprotection mechanism in cyanobacteria by incorporating a watermarked FSRS version to address the large and sometimes unpredictable spectral baseline issues. Ancestral to the aforementioned plant-like LHC to capture incoming photons, the cyanobacterial photosynthetic system uses the high-light inducible proteins (Hlips), including HliC and HliD, which have been isolated and considered to bind four or six chlorophyll *a* (Chl *a*, a specific form of green pigment) and two β-carotenes per one putative dimer. Once again, FSRS affords an effective methodology to tackle the controversial mechanistic origin of excited-state chlorophyll quenching by carotenoids. One novel aspect of this work is the application of tunable FSRS to monitor energy transfer in a photosynthetic LHC through pigment–protein or pigment–pigment interactions. Aided by TA spectroscopy, the Kennis group tracked vibrations with sub-100-fs time resolution during the HliC quenching (131). The actinic-pump-dependent FSRS peak frequency variation uncovers at least two distinct β-carotenes with effective conjugation lengths of ∼10.5 (β-car$_2$) and 9.6 (β-car$_1$), the former conformation acting as the main quenching site due to its electronic energy state lowering by up to 800 cm^{-1}. Notably, spectral watermarking has also been applied to photosensitive biomolecules such as the Na^+ pump rhodopsin (132). These studies have laid solid groundwork to implement FSRS for more general photosynthesis research. Moreover, the photoprotection mechanism via intermolecular-interaction-induced excited-state energy tuning and directional energy flow from Chl *a* to β-carotene on 2- and 30-ps timescales (131) has contributed to our increased understanding of photoprotection mechanisms in DNA bases and derivatives (39, 133), sunscreens (134), and organic chromophores (42).

Another hallmark example for energy transfer in biology concerns heme proteins (93, 135). Myoglobin (Mb) is a cytoplasmic iron- and oxygen-binding monomeric hemoprotein with a heme group consisting of a protoporphyrin chromophore and an iron atom at its center. The organic cofactor includes four pyrrole rings linked by methine bridges, structurally similar to the bilin chromophore in phytochromes (13). The heme has an extremely short nonradiative excited-state lifetime on the femtosecond timescale, leading to excess vibrational energy above 20,000 cm^{-1} to be optically deposited at the heme site. The main research interests on heme proteins have concentrated on the photoinduced heme coordinating state and structural changes on ultrafast timescales; the interactions between heme, protein residues, and ligands; and vibrational energy relaxation and propagation in heme via the protein moiety to solution on longer timescales (87, 136–139).

Recently, FSRS reports appeared for protein dynamics and energy flow in metMb (the ferric form of the protein) (58) as well as Mb (the ferrous state) (21, 23) in its carbonmonoxy (MbCO) and deoxy (deoxy-Mb) forms. Related studies benefited from a broadly tunable picosecond Raman pump from 350 to 600 nm with spectral shaping (140), achieving resonance FSRS in the typically challenging blue-wavelength region (48, 51, 59, 141). After pumping the Q band at 560 nm and performing stimulated Raman around the Soret band at ∼430 nm of Mb, Scopigno and coworkers (21) studied the temporal evolution of different vibrational modes (**Figure 6**). Spectral analysis aided by fs-TA and numerical model calculations reveals that efficient vibrational energy transfer out of the highly excited FC manifold into low- and high-frequency modes (**Figure 6*a*,*b***) occurs

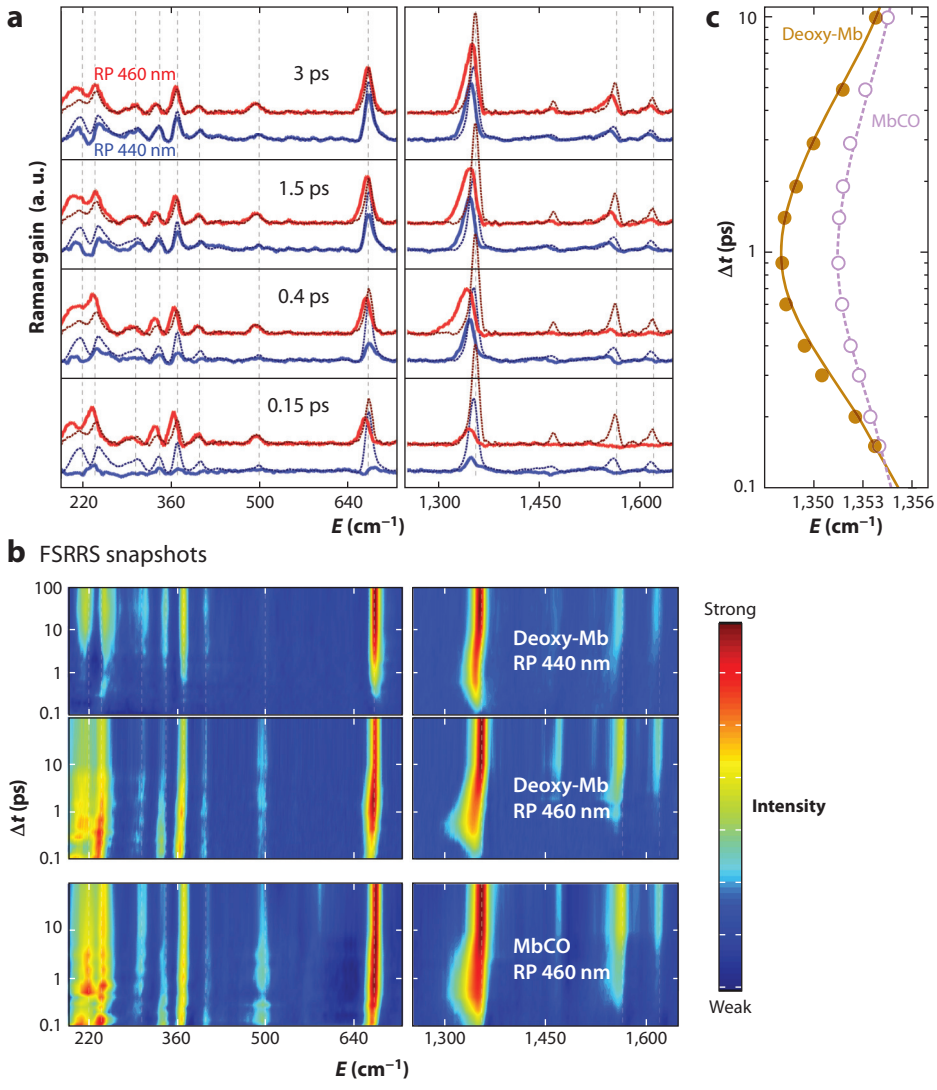

Figure 6

Tunable resonance FSRS (termed FSRRS) tracks vibrational energy flow on ultrafast timescales: an example using myoglobin. (*a*) Time-resolved FSRS spectra of deoxy-Mb (*solid curves*) and reference without actinic pump (*dashed curves*) with RP at 440 nm (*blue*) and 460 nm (*red*). (*b*) Contour maps associated with panel *a*. The color bar shows strong to weak intensities from red to blue, respectively. (*c*) Kinetic plot of the ~1,355-cm^{-1} Raman mode frequency, *E*, after 560-nm photoexcitation for deoxy-Mb (*brown curve*) and MbCO (*purple dashed curve*) with biexponentially fitted ~0.3- and 6-ps time constants. Figure adapted from Reference 21 with permission; copyright 2016 Macmillan Publishers Ltd: Nature Chemistry, part of Springer Nature. Abbreviations: FSRS, femtosecond stimulated Raman spectroscopy; MbCO, myoglobin bound with carbon monoxide or carbonmonoxy myoglobin; RP, Raman pump.

on faster and slower timescales, respectively. Initial nonradiative transition from the Q band to the highly excited ground-state vibronic manifold occurs on the ~300-fs timescale (142), followed by vibrational cooling on the ~3-ps timescale. Vibrational heating and cooling are more prominent with a larger amplitude of frequency shift in deoxy-Mb than MbCO (**Figure 6*c***), because MbCO

needs to consume some photoexcitation energy for ligand dissociation. The proposed mechanism thus involved only hot ground-state relaxation (93), without the need to invoke some transient electronic intermediates or setting an upper limit for their lifetime to be ~50 fs (21).

Scopigno and coworkers' experiment used a 440- and 460-nm Raman pump to selectively track the ground- and higher-lying vibrational states of Mb in S_0 with different photoinduced mode frequency-shift patterns (21, 23), highlighting the unique power of tunable FSRS to achieve different resonance conditions and track various species or states with femtosecond resolution (see Section 2.4) (17, 35, 38, 52, 59). This work also represents a unique experimental scenario in that the actinic pump (i.e., within the ground-state, lower-energy absorption band) is located to the red side of the Raman pump–probe pair (i.e., within the ground-state, higher-energy absorption band), which may involve additional Feynman diagrams and complex line shapes in the resonance FSRS signal generation (see **Figures 1** and **2** for the relationship between FSRS laser pulses and PESs; also see Section 2.2) (34–36, 49, 54, 56, 69).

4. CONCLUDING REMARKS AND PROSPECTS

In this review, we have followed the recent development of FSRS as a versatile and powerful technique to map structural dynamics of proteins. Since the early 2000s, more research labs have joined forces to elevate the paradigm-shift FSRS field to new heights (9, 12, 14, 32, 34, 52). Meanwhile, Raman spectroscopy as a whole has enjoyed a renaissance and has been developed into an almost universally applicable analytical technique (2, 10, 16, 65, 137, 143–145), which also comprises stimulated Raman scattering microscopy (145–150). The expanding tool set includes (*a*) wavelength coverage from the NIR to deep UV, (*b*) efficient light conversion via both home-built and commercial setups, (*c*) spectral data collection in either the mixed time-frequency domain or purely the time domain, and (*d*) selective sensitivity to the chromophore and surrounding protein residues. Theoretical efforts have greatly contributed to deepening our understanding of how FSRS works in the electronic ground and excited states, how Raman peak line shapes vary when approaching electronic resonances (36, 49, 67, 72), and how FSRS spectral changes track the conformational dynamics in real time with site specificity and high resolution.

On the sample front, as large complex organic materials, proteins are anharmonic and display vibrational signatures on many decades of timescales. Sophisticated organic and biochemical methods to precisely incorporate isotopic labels and functional groups (41, 75, 151), mutations (24, 112), and noncanonical amino acids (152, 153) into proteins have started to enable a systematic evaluation of functionality change. Fittingly, FSRS provides a highly sensitive and nondestructive platform to capture structural snapshots of proteins, particularly for light-sensitive proteins in H-bonding environments (34, 52, 88). The correlation between existing knowledge on proteins (from steady-state, time-resolved X-ray crystallography as well as electronic and IR spectroscopy) and new knowledge gained by FSRS investigations is synergistic; despite their drawbacks with experimental mitigation strategies (Section 2.5), they nicely complement each other (55). Though FSRS as a spectroscopic method does not give direct structural data [information that can be obtained by ultrafast X-ray and electron diffraction methods (154, 155)], the spectroscopic information gained from a tabletop FSRS setup may allow for deriving how various proteins work in real time (see Section 3). This rationale highlights the need to delineate the structure–function relationships of proteins with a combination of advanced techniques, including the time-resolved X-ray, electronic, and vibrational spectroscopies that are still being actively developed.

Looking forward, seeking a deeper understanding of chemical reactivity in proteins will continue to motivate FSRS studies on colorful FPs and FP-based biosensors, photoreceptor proteins with diverse functions, and proteins with optogenetic capabilities (109). Distinct protein functions

under various conditions pose experimental challenges from sample photostability to SNR and tracking transient species to functional relevance of spectral data (i.e., there is no one-size-fits-all approach). The relevance of retrieved low-frequency motions and vibrational oscillations in 2D-FSRS remains a hot topic because of the apparent mismatch between pertinent timescales (shorter for low-frequency coherent motions but longer for photochemical reactions such as ESPT; see Section 3.1), which can be further investigated by comparative studies on similar protein systems with strategic mutations or noncanonical amino acids to alter functions (24, 52, 94, 114, 153), as well as related systems with well-defined structural differences but similar functions (2, 16). With tunability of individual femtosecond- and picosecond-laser pulses across a wide range, the application prospects and accessibility of FSRS have been enormously broadened, with richer information being attained on a regular basis even for complex environments such as those inside proteins.

Specifically, previously hidden nuclear motions and molecular species that accompany or control chemical reactivity will be unveiled, one coordinate at a time, and simultaneous tracking of multiple vibrational marker bands remains an essential strategy to map the multidimensional reaction coordinates with a directed outcome. This broadband spectral coverage with readily incorporated time-resolved capability will continue to benefit from the development of more stable white-light probes into the UV and IR regions (42, 48, 59, 61, 62, 141). Moreover, such mechanistic insights on the molecular level have started to enable targeted design of proteins as shown for the FP-based calcium biosensor with distinct fluorescence outcomes (see Section 3.1.3). Close synergy between spectroscopic and theoretical groups has already demonstrated its power in tackling some of the most pressing problems in the protein structural dynamics field (56, 60, 69, 88, 94, 109). On a broader note, in comparison to microscopy, spectroscopy is currently underrated and could benefit from more enthusiastic and motivated scientists, researchers, and young minds. We envision that the real-time visualization and fundamental understanding of photoinduced transient species and functional skeletal motions alike will greatly enhance collaborations between spectroscopists, theoreticians, protein engineers, and life scientists to make a broader impact with more exciting discoveries and tangible societal benefits.

SUMMARY POINTS

1. FSRS methodology with broadly tunable ultrafast laser pulses enables the real-time tracking of photophysical and photochemical processes inside proteins, particularly around the photosensory unit (active site) from the reactant to product states.
2. Transient absorption spectroscopy acts as an effective precursor to FSRS experiments in selecting optimal laser wavelengths and achieving dynamic resonance enhancement of the molecular or chemical species of interest.
3. Mode-specific FSRS line shapes are governed by resonance conditions sensed by individual vibrational modes across a broad spectral region, which help dissect the multidimensional PES upon tuning both the actinic-pump and Raman-pump wavelengths.
4. Excited-state proton transfer inside a protein matrix represents a prime example to optimize tunable FSRS setups in tracking proton movement on ultrafast timescales while unveiling functional structural motions during a photochemical reaction.
5. Structural dynamics mapping by tunable FSRS provides rigorous benchmarks and molecular insights to enable rational design at the site-specific level with targeted functional group substitutions.

DISCLOSURE STATEMENT

The authors are not aware of any affiliations, memberships, funding, or financial holdings that might be perceived as affecting the objectivity of this review.

ACKNOWLEDGMENTS

This work was supported by an NSF CAREER grant (CHE-1455353), an Oregon Medical Research Foundation New Investigator Grant (2016–2017), an Oregon State University Faculty Research Start-Up Grant (2010–2016), and the Research Equipment Reserve Fund (spring 2014) to C.F. The authors thank their current and former group members, in particular Dr. Weimin Liu, Dr. Liangdong Zhu, Dr. Fangyuan Han, Dr. Breland Oscar, Dr. Yanli Wang, Cheng Chen, Sean Tachibana, and Taylor Krueger.

LITERATURE CITED

1. Boehr DD, Nussinov R, Wright PE. 2009. The role of dynamic conformational ensembles in biomolecular recognition. *Nat. Chem. Biol.* 5:789–96
2. **Fang C, Frontiera RR, Tran R, Mathies RA. 2009. Mapping GFP structure evolution during proton transfer with femtosecond Raman spectroscopy. *Nature* 462:200–4**
3. Cho HS, Schotte F, Dashdorj N, Kyndt J, Henning R, Anfinrud PA. 2016. Picosecond photobiology: watching a signaling protein function in real time via time-resolved small- and wide-angle X-ray scattering. *J. Am. Chem. Soc.* 138:8815–23
4. Ghosh A, Ostrander JS, Zanni MT. 2017. Watching proteins wiggle: mapping structures with two-dimensional infrared spectroscopy. *Chem. Rev.* 117:10726–59
5. Hochstrasser RM. 2007. Two-dimensional spectroscopy at infrared and optical frequencies. *PNAS* 104:14190–96
6. Vos MH, Rappaport F, Lambry J-C, Breton J, Martin J-L. 1993. Visualization of coherent nuclear motion in a membrane protein by femtosecond spectroscopy. *Nature* 363:320–25
7. Zewail AH. 1994. *Femtochemistry: Ultrafast Dynamics of the Chemical Bond*. Singapore: World Sci.
8. Johnson PJM, Farag MH, Halpin A, Morizumi T, Prokhorenko VI, et al. 2017. The primary photochemistry of vision occurs at the molecular speed limit. *J. Phys. Chem. B* 121:4040–47
9. Hoffman DP, Mathies RA. 2016. Femtosecond stimulated Raman exposes the role of vibrational coherence in condensed-phase photoreactivity. *Acc. Chem. Res.* 49:616–25
10. Kukura P, McCamant DW, Yoon S, Wandschneider DB, Mathies RA. 2005. Structural observation of the primary isomerization in vision with femtosecond-stimulated Raman. *Science* 310:1006–9
11. McCamant DW, Kukura P, Mathies RA. 2005. Femtosecond stimulated Raman study of excited-state evolution in bacteriorhodopsin. *J. Phys. Chem. B* 109:10449–57
12. Kukura P, McCamant DW, Mathies RA. 2007. Femtosecond stimulated Raman spectroscopy. *Annu. Rev. Phys. Chem.* 58:461–88
13. Dasgupta J, Frontiera RR, Taylor KC, Lagarias JC, Mathies RA. 2009. Ultrafast excited-state isomerization in phytochrome revealed by femtosecond stimulated Raman spectroscopy. *PNAS* 106:1784–89
14. Frontiera RR, Fang C, Dasgupta J, Mathies RA. 2012. Probing structural evolution along multidimensional reaction coordinates with femtosecond stimulated Raman spectroscopy. *Phys. Chem. Chem. Phys.* 14:405–14
15. Nakamura R, Hamada N, Abe K, Yoshizawa M. 2012. Ultrafast hydrogen-bonding dynamics in the electronic excited state of photoactive yellow protein revealed by femtosecond stimulated Raman spectroscopy. *J. Phys. Chem. B* 116:14768–75
16. **Oscar BG, Liu W, Zhao Y, Tang L, Wang Y, et al. 2014. Excited-state structural dynamics of a dual-emission calmodulin-green fluorescent protein sensor for calcium ion imaging. *PNAS* 111:10191–96**

2. Groundbreaking report of FSRS on wild-type GFP with an intrinsic 2D-FSRS approach.

16. First application of FSRS on FP-based calcium biosensors, uncovering a functional low-frequency mode different from wild-type GFP.

17. Tang L, Liu W, Wang Y, Zhao Y, Oscar BG, et al. 2015. Unraveling ultrafast photoinduced proton transfer dynamics in a fluorescent protein biosensor for Ca^{2+} imaging. *Chem. Eur. J.* 21:6481–90

18. Wang Y, Tang L, Liu W, Zhao Y, Oscar BG, et al. 2015. Excited state structural events of a dual-emission fluorescent protein biosensor for Ca^{2+} imaging studied by femtosecond stimulated Raman spectroscopy. *J. Phys. Chem. B* 119:2204–18

19. Tang L, Liu W, Wang Y, Zhu L, Han F, Fang C. 2016. Ultrafast structural evolution and chromophore inhomogeneity inside a green-fluorescent-protein-based Ca^{2+} biosensor. *J. Phys. Chem. Lett.* 7:1225–30

20. Schnedermann C, Muders V, Ehrenberg D, Schlesinger R, Kukura P, Heberle J. 2016. Vibronic dynamics of the ultrafast all-*trans* to 13-*cis* photoisomerization of retinal in Channelrhodopsin-1. *J. Am. Chem. Soc.* 138:4757–62

21. Ferrante C, Pontecorvo E, Cerullo G, Vos MH, Scopigno T. 2016. Direct observation of subpicosecond vibrational dynamics in photoexcited myoglobin. *Nat. Chem.* 8:1137–43

22. Fujisawa T, Kuramochi H, Hosoi H, Takeuchi S, Tahara T. 2016. Role of coherent low-frequency motion in excited-state proton transfer of green fluorescent protein studied by time-resolved impulsive stimulated Raman spectroscopy. *J. Am. Chem. Soc.* 138:3942–45

23. Batignani G, Pontecorvo E, Giovannetti G, Ferrante C, Fumero G, Scopigno T. 2016. Electronic resonances in broadband stimulated Raman spectroscopy. *Sci. Rep.* 6:18445

24. Tachibana SR, Tang L, Wang Y, Zhu L, Liu W, Fang C. 2017. Tuning calcium biosensors with a single-site mutation: structural dynamics insights from femtosecond Raman spectroscopy. *Phys. Chem. Chem. Phys.* 19:7138–46

25. Tang L, Wang Y, Liu W, Zhao Y, Campbell RE, Fang C. 2017. Illuminating photochemistry of an excitation ratiometric fluorescent protein calcium biosensor. *J. Phys. Chem. B* 121:3016–23

26. Kuramochi H, Takeuchi S, Yonezawa K, Kamikubo H, Kataoka M, Tahara T. 2017. Probing the early stages of photoreception in photoactive yellow protein with ultrafast time-domain Raman spectroscopy. *Nat. Chem.* 9:660–66

27. Tachibana SR, Tang L, Zhu L, Liu W, Wang Y, Fang C. 2018. Watching an engineered calcium biosensor glow: altered reaction pathways before emission. *J. Phys. Chem. B* 122:11986–95

28. Tang L, Zhu L, Taylor MA, Wang Y, Remington SJ, Fang C. 2018. Excited state structural evolution of a GFP single-site mutant tracked by tunable femtosecond-stimulated Raman spectroscopy. *Molecules* 23:2226

29. Frontiera RR, Dasgupta J, Mathies RA. 2009. Probing interfacial electron transfer in Coumarin 343 sensitized TiO_2 nanoparticles with femtosecond stimulated Raman. *J. Am. Chem. Soc.* 131:15630–32

30. Provencher F, Bérubé N, Parker AW, Greetham GM, Towrie M, et al. 2014. Direct observation of ultrafast long-range charge separation at polymer-fullerene heterojunctions. *Nat. Commun.* 5:4288

31. Hoffman DP, Ellis SR, Mathies RA. 2014. Characterization of a conical intersection in a charge-transfer dimer with two-dimensional time-resolved stimulated Raman spectroscopy. *J. Phys. Chem. A* 118:4955–65

32. Bragg AE, Yu W, Zhou J, Magnanelli T. 2016. Ultrafast Raman spectroscopy as a probe of local structure and dynamics in photoexcited conjugated materials. *J. Phys. Chem. Lett.* 7:3990–4000

33. Tang L, Zhu L, Ener ME, Gao H, Wang Y, et al. 2019. Photoinduced charge flow inside an iron porphyrazine complex. *Chem. Commun.* 55:13606–9

34. Dietze DR, Mathies RA. 2016. Femtosecond stimulated Raman spectroscopy. *ChemPhysChem* 17:1224–51

35. Liu W, Tang L, Oscar BG, Wang Y, Chen C, Fang C. 2017. Tracking ultrafast vibrational cooling during excited state proton transfer reaction with anti-Stokes and Stokes femtosecond stimulated Raman spectroscopy. *J. Phys. Chem. Lett.* 8:997–1003

36. Oscar BG, Chen C, Liu W, Zhu L, Fang C. 2017. Dynamic Raman line shapes on an evolving excited-state landscape: insights from tunable femtosecond stimulated Raman spectroscopy. *J. Phys. Chem. A* 121:5428–41

37. Zhu L, Liu W, Fang C. 2014. A versatile femtosecond stimulated Raman spectroscopy setup with tunable pulses in the visible to near infrared. *Appl. Phys. Lett.* 105:041106

17. First report of tunable FSRS on FP-based biosensors, demonstrating feasibility of tracking transient molecular species in proteins.

21. Demonstrates power of resonance FSRS to track mode-specific vibrational cooling and energy redistribution in heme proteins.

28. First application of anti-Stokes FSRS with tunable Raman pump on proteins.

34. Comprehensive review on FSRS history, technical advances, and various applications up to 2016.

36. Introduces dynamic mode-specific line shapes in anti-Stokes FSRS of a photoexcited chromophore in solution.

37. First technical report on an integrated tunable FSRS setup with BUMA as the Raman probe.

38. Liu W, Wang Y, Tang L, Oscar BG, Zhu L, Fang C. 2016. Panoramic portrait of primary molecular events preceding excited state proton transfer in water. *Chem. Sci.* 7:5484–94

39. Lee J, Challa JR, McCamant DW. 2017. Ultraviolet light makes dGMP floppy: femtosecond stimulated Raman spectroscopy of 2′-deoxyguanosine 5′-monophosphate. *J. Phys. Chem. B* 121:4722–32
40. Roy K, Kayal S, Ariese F, Beeby A, Umapathy S. 2017. Mode specific excited state dynamics study of bis(phenylethynyl)benzene from ultrafast Raman loss spectroscopy. *J. Chem. Phys.* 146:064303
41. Chen C, Liu W, Baranov MS, Baleeva NS, Yampolsky IV, et al. 2017. Unveiling structural motions of a highly fluorescent superphotoacid by locking and fluorinating the GFP chromophore in solution. *J. Phys. Chem. Lett.* 8:5921–28
42. Tang L, Wang Y, Zhu L, Lee C, Fang C. 2018. Correlated molecular structural motions for photoprotection after deep-UV irradiation. *J. Phys. Chem. Lett.* 9:2311–19
43. Westlake BC, Brennaman MK, Concepcion JJ, Paul JJ, Bettis SE, et al. 2011. Concerted electron-proton transfer in the optical excitation of hydrogen-bonded dyes. *PNAS* 108:8554–58
44. Han F, Liu W, Fang C. 2013. Excited-state proton transfer of photoexcited pyranine in water observed by femtosecond stimulated Raman spectroscopy. *Chem. Phys.* 422:204–19
45. Yang KR, Xu X, Zheng J, Truhlar DG. 2014. Full-dimensional potentials and state couplings and multidimensional tunneling calculations for the photodissociation of phenol. *Chem. Sci.* 5:4661–80
46. Yoshizawa M, Kurosawa M. 1999. Femtosecond time-resolved Raman spectroscopy using stimulated Raman scattering. *Phys. Rev. A* 61:013808
47. McCamant DW, Kukura P, Yoon S, Mathies RA. 2004. Femtosecond broadband stimulated Raman spectroscopy: apparatus and methods. *Rev. Sci. Instrum.* 75:4971–80
48. Laimgruber S, Schachenmayr H, Schmidt B, Zinth W, Gilch P. 2006. A femtosecond stimulated Raman spectrograph for the near ultraviolet. *Appl. Phys. B* 85:557–64
49. Weigel A, Dobryakov A, Klaumünzer B, Sajadi M, Saalfrank P, Ernsting NP. 2011. Femtosecond stimulated Raman spectroscopy of flavin after optical excitation. *J. Phys. Chem. B* 115:3656–80
50. Wang W, Liu W, Chang I-Y, Wills LA, Zakharov LN, et al. 2013. Electrolytic synthesis of aqueous aluminum nanoclusters and in situ characterization by femtosecond Raman spectroscopy and computations. *PNAS* 110:18397–401
51. Zhu L, Saha S, Wang Y, Keszler DA, Fang C. 2016. Monitoring photochemical reaction pathways of tungsten hexacarbonyl in solution from femtoseconds to minutes. *J. Phys. Chem. B* 120:13161–68

52. Fang C, Tang L, Oscar BG, Chen C. 2018. Capturing structural snapshots during photochemical reactions with ultrafast Raman spectroscopy: from materials transformation to biosensor responses. *J. Phys. Chem. Lett.* 9:3253–63

53. Liu W, Han F, Smith C, Fang C. 2012. Ultrafast conformational dynamics of pyranine during excited state proton transfer in aqueous solution revealed by femtosecond stimulated Raman spectroscopy. *J. Phys. Chem. B* 116:10535–50
54. Dorfman KE, Fingerhut BP, Mukamel S. 2013. Time-resolved broadband Raman spectroscopies: a unified six-wave-mixing representation. *J. Chem. Phys.* 139:124113
55. Fang C, Tang L, Chen C. 2019. Unveiling coupled electronic and vibrational motions of chromophores in condensed phase. *J. Chem. Phys.* 151:200901
56. Lee S-Y, Zhang D, McCamant DW, Kukura P, Mathies RA. 2004. Theory of femtosecond stimulated Raman spectroscopy. *J. Chem. Phys.* 121:3632–42
57. Zhu L, Liu W, Fang C. 2013. Tunable sideband laser from cascaded four-wave mixing in thin glass for ultra-broadband femtosecond stimulated Raman spectroscopy. *Appl. Phys. Lett.* 103:061110
58. Molesky BP, Guo Z, Moran AM. 2015. Femtosecond stimulated Raman spectroscopy by six-wave mixing. *J. Chem. Phys.* 142:212405
59. Zhu L, Liu W, Wang Y, Fang C. 2015. Sum-frequency-generation-based laser sidebands for tunable femtosecond Raman spectroscopy in the ultraviolet. *Appl. Sci.* 5:48–61
60. Monacelli L, Batignani G, Fumero G, Ferrante C, Mukamel S, Scopigno T. 2017. Manipulating impulsive stimulated Raman spectroscopy with a chirped probe pulse. *J. Phys. Chem. Lett.* 8:966–74
61. Liu W, Zhu L, Fang C. 2012. Observation of sum-frequency-generation-induced cascaded four-wave mixing using two crossing femtosecond laser pulses in a 0.1 mm beta-barium-borate crystal. *Opt. Lett.* 37:3783–85

38. Tunable FSRS-enabled direct tracking of low-frequency modes and coherent oscillations of organic chromophores in water.

52. Recent perspective on tunable FSRS development and implementations for biological and materials science and engineering.

62. Liu W, Zhu L, Wang L, Fang C. 2013. Cascaded four-wave mixing for broadband tunable laser sideband generation. *Opt. Lett.* 38:1772–74
63. Han F, Liu W, Zhu L, Wang Y, Fang C. 2016. Initial hydrogen-bonding dynamics of photoexcited coumarin in solution with femtosecond stimulated Raman spectroscopy. *J. Mater. Chem. C* 4:2954–63
64. Yan Y-X, Gamble EB, Nelson KA. 1985. Impulsive stimulated scattering: general importance in femtosecond laser pulse interactions with matter, and spectroscopic applications. *J. Chem. Phys.* 83:5391–99
65. Takeuchi S, Ruhman S, Tsuneda T, Chiba M, Taketsugu T, Tahara T. 2008. Spectroscopic tracking of structural evolution in ultrafast stilbene photoisomerization. *Science* 322:1073–77
66. Johnson PJM, Halpin A, Morizumi T, Prokhorenko VI, Ernst OP, Miller RJD. 2015. Local vibrational coherences drive the primary photochemistry of vision. *Nat. Chem.* 7:980–86
67. Rao BJ, Gelin MF, Domcke W. 2016. Resonant femtosecond stimulated Raman spectra: theory and simulations. *J. Phys. Chem. A* 120:3286–95
68. Dean JC, Mirkovic T, Toa ZSD, Oblinsky DG, Scholes GD. 2016. Vibronic enhancement of algae light harvesting. *Chem* 1:858–72
69. Batignani G, Fumero G, Mukamel S, Scopigno T. 2015. Energy flow between spectral components in 2D broadband stimulated Raman spectroscopy. *Phys. Chem. Chem. Phys.* 17:10454–61
70. Wang L, Liu W, Fang C. 2015. Elucidating low-frequency vibrational dynamics in calcite and water with time-resolved third-harmonic generation spectroscopy. *Phys. Chem. Chem. Phys.* 17:17034–40
71. Quick M, Dobryakov AL, Kovalenko SA, Ernsting NP. 2015. Resonance femtosecond-stimulated Raman spectroscopy without actinic excitation showing low-frequency vibrational activity in the S_2 state of all-trans β-carotene. *J. Phys. Chem. Lett.* 6:1216–20
72. Chen C, Zhu L, Fang C. 2018. Femtosecond stimulated Raman line shapes: dependence on resonance conditions of pump and probe pulses. *Chin. J. Chem. Phys.* 31:492–502
73. Liebel M, Schnedermann C, Wende T, Kukura P. 2015. Principles and applications of broadband impulsive vibrational spectroscopy. *J. Phys. Chem. A* 119:9506–17
74. Hamm P, Lim M, Hochstrasser RM. 1998. Structure of the amide I band of peptides measured by femtosecond nonlinear-infrared spectroscopy. *J. Phys. Chem. B* 102:6123–38
75. Fang C, Wang J, Charnley AK, Barber-Armstrong W, Smith AB III, et al. 2003. Two-dimensional infrared measurements of the coupling between amide modes of an α-helix. *Chem. Phys. Lett.* 382:586–92
76. Zheng J, Kwak K, Asbury J, Chen X, Piletic IR, Fayer MD. 2005. Ultrafast dynamics of solute-solvent complexation observed at thermal equilibrium in real time. *Science* 309:1338–43
77. Fang C, Senes A, Cristian L, DeGrado WF, Hochstrasser RM. 2006. Amide vibrations are delocalized across the hydrophobic interface of a transmembrane helix dimer. *PNAS* 103:16740–45
78. Fang C, Bauman JD, Das K, Remorino A, Arnold E, Hochstrasser RM. 2008. Two-dimensional infrared spectra reveal relaxation of the nonnucleoside inhibitor TMC278 complexed with the HIV-1 reverse transcriptase. *PNAS* 105:1472–77
79. Kratochvil HT, Carr JK, Matulef K, Annen AW, Li H, et al. 2016. Instantaneous ion configurations in the K^+ ion channel selectivity filter revealed by 2D IR spectroscopy. *Science* 353:1040–44
80. Zhao B, Sun Z, Lee S-Y. 2011. Quantum theory of time-resolved femtosecond stimulated Raman spectroscopy: direct versus cascade processes and application to $CDCl_3$. *J. Chem. Phys.* 134:024307
81. Dunlap B, Wilson KC, McCamant DW. 2013. Phase-matching and dilution effects in two-dimensional femtosecond stimulated Raman spectroscopy. *J. Phys. Chem. A* 117:6205–16
82. Tonge PJ, Meech SR. 2009. Excited state dynamics in the green fluorescent protein. *J. Photochem. Photobiol. A Chem.* 205:1–11
83. Meech SR. 2009. Excited state reactions in fluorescent proteins. *Chem. Soc. Rev.* 38:2922–34
84. Polli D, Altoè P, Weingart O, Spillane KM, Manzoni C, et al. 2010. Conical intersection dynamics of the primary photoisomerization event in vision. *Nature* 467:440–43
85. Hall CR, Conyard J, Heisler IA, Jones G, Frost J, et al. 2017. Ultrafast dynamics in light-driven molecular rotary motors probed by femtosecond stimulated Raman spectroscopy. *J. Am. Chem. Soc.* 139:7408–14
86. Taylor MA, Zhu L, Rozanov ND, Stout KT, Chen C, Fang C. 2019. Delayed vibrational modulation of the solvated GFP chromophore into a conical intersection. *Phys. Chem. Chem. Phys.* 21:9728–39

87. Lian T, Locke B, Kholodenko Y, Hochstrasser RM. 1994. Energy flow from solute to solvent probed by femtosecond IR spectroscopy: malachite green and heme protein solutions. *J. Phys. Chem.* 98:11648–56
88. Laage D, Elsaesser T, Hynes JT. 2017. Water dynamics in the hydration shells of biomolecules. *Chem. Rev.* 117:10694–725
89. Frauenfelder H, Sligar SG, Wolynes PG. 1991. The energy landscapes and motions of proteins. *Science* 254:1598–603
90. Feynman RP. 1970. *The Feynman Lectures on Physics*. Boston, MA: Addison Wesley Longman
91. Chattoraj M, King BA, Bublitz GU, Boxer SG. 1996. Ultra-fast excited state dynamics in green fluorescent protein: multiple states and proton transfer. *PNAS* 93:8362–67
92. Brejc K, Sixma TK, Kitts PA, Kain SR, Tsien RY, et al. 1997. Structural basis for dual excitation and photoisomerization of the *Aequorea victoria* green fluorescent protein. *PNAS* 94:2306–11
93. Champion PM. 2005. Following the flow of energy in biomolecules. *Science* 310:980–82
94. Schnedermann C, Yang X, Liebel M, Spillane KM, Lugtenburg J, et al. 2018. Evidence for a vibrational phase-dependent isotope effect on the photochemistry of vision. *Nat. Chem.* 10:449–55
95. Chen C, Zhu L, Baranov MS, Tang L, Baleeva NS, et al. 2019. Photoinduced proton transfer of GFP-inspired fluorescent superphotoacids: principles and design. *J. Phys. Chem. B* 123:3804–21
96. Cellmer T, Buscaglia M, Henry ER, Hofrichter J, Eaton WA. 2011. Making connections between ultrafast protein folding kinetics and molecular dynamics simulations. *PNAS* 108:6103–8
97. Zimmer M. 2002. Green fluorescent protein (GFP): applications, structure, and related photophysical behavior. *Chem. Rev.* 102:759–81
98. Tsien RY. 1998. The green fluorescent protein. *Annu. Rev. Biochem.* 67:509–44
99. Shimomura O, Johnson FH, Saiga Y. 1962. Extraction, purification and properties of Aequorin, a bioluminescent protein from the luminous hydromedusan, *Aequorea*. *J. Cell. Comp. Physiol.* 59:223–39
100. Chalfie M, Tu Y, Euskirchen G, Ward WW, Prasher DC. 1994. Green fluorescent protein as a marker for gene expression. *Science* 263:802–5
101. Miyawaki A, Llopis J, Heim R, McCaffery JM, Adams JA, et al. 1997. Fluorescent indicators for Ca^{2+} based on green fluorescent proteins and calmodulin. *Nature* 388:882–87
102. Ormo M, Cubitt AB, Kallio K, Gross LA, Tsien RY, Remington SJ. 1996. Crystal structure of the *Aequorea victoria* green fluorescent protein. *Science* 273:1392–95
103. Kennis JTM, Larsen DS, van Stokkum IHM, Vengris M, van Thor JJ, van Grondelle R. 2004. Uncovering the hidden ground state of green fluorescent protein. *PNAS* 101:17988–93
104. Zhao Y, Araki S, Wu J, Teramoto T, Chang Y-F, et al. 2011. An expanded palette of genetically encoded Ca^{2+} indicators. *Science* 333:1888–91
105. Wang Q, Shui B, Kotlikoff MI, Sondermann H. 2008. Structural basis for calcium sensing by GCaMP2. *Structure* 16:1817–27
106. Akerboom J, Rivera JDV, Guilbe MMR, Malavé ECA, Hernandez HH, et al. 2009. Crystal structures of the GCaMP calcium sensor reveal the mechanism of fluorescence signal change and aid rational design. *J. Biol. Chem.* 284:6455–64
107. Pédelacq J-D, Cabantous S, Tran T, Terwilliger TC, Waldo GS. 2005. Engineering and characterization of a superfolder green fluorescent protein. *Nat. Biotechnol.* 24:79–88
108. Petrone A, Cimino P, Donati G, Hratchian HP, Frisch MJ, Rega N. 2016. On the driving force of the excited-state proton shuttle in the green fluorescent protein: a time-dependent density functional theory (TD-DFT) study of the intrinsic reaction path. *J. Chem. Theory Comput.* 12:4925–33
109. Scholes GD, Fleming GR, Chen LX, Aspuru-Guzik A, Buchleitner A, et al. 2017. Using coherence to enhance function in chemical and biophysical systems. *Nature* 543:647–56
110. Park JW, Rhee YM. 2016. Electric field keeps chromophore planar and produces high yield fluorescence in green fluorescent protein. *J. Am. Chem. Soc.* 138:13619–29
111. Conyard J, Heisler IA, Chan Y, Bulman Page PC, Meech SR, Blancafort L. 2018. A new twist in the photophysics of the GFP chromophore: a volume-conserving molecular torsion couple. *Chem. Sci.* 9:1803–12
112. Tang L, Wang Y, Zhu L, Kallio K, Remington SJ, Fang C. 2018. Photoinduced proton transfer inside an engineered green fluorescent protein: a stepwise-concerted-hybrid reaction. *Phys. Chem. Chem. Phys.* 20:12517–26

113. Schnedermann C, Liebel M, Kukura P. 2015. Mode-specificity of vibrationally coherent internal conversion in rhodopsin during the primary visual event. *J. Am. Chem. Soc.* 137:2886–91
114. Liebel M, Kukura P. 2017. Lack of evidence for phase-only control of retinal photoisomerization in the strict one-photon limit. *Nat. Chem.* 9:45–49
115. Chudakov DM, Belousov VV, Zaraisky AG, Novoselov VV, Staroverov DB, et al. 2003. Kindling fluorescent proteins for precise in vivo photolabeling. *Nat. Biotechnol.* 21:191–94
116. Henderson JN, Ai HW, Campbell RE, Remington SJ. 2007. Structural basis for reversible photobleaching of a green fluorescent protein homologue. *PNAS* 104:6672–77
117. Zhou XX, Lin MZ. 2013. Photoswitchable fluorescent proteins: ten years of colorful chemistry and exciting applications. *Curr. Opin. Chem. Biol.* 17:682–90
118. Acharya A, Bogdanov AM, Grigorenko BL, Bravaya KB, Nemukhin AV, et al. 2016. Photoinduced chemistry in fluorescent proteins: curse or blessing? *Chem. Rev.* 117:758–95
119. Stiel AC, Trowitzsch S, Weber G, Andresen M, Eggeling C, et al. 2007. 1.8 Å bright-state structure of the reversibly switchable fluorescent protein Dronpa guides the generation of fast switching variants. *Biochem. J.* 402:35–42
120. Mizuno H, Mal TK, Walchli M, Kikuchi A, Fukano T, et al. 2008. Light-dependent regulation of structural flexibility in a photochromic fluorescent protein. *PNAS* 105:9227–32
121. Fron E, Flors C, Schweitzer G, Habuchi S, Mizuno H, et al. 2007. Ultrafast excited-state dynamics of the photoswitchable protein Dronpa. *J. Am. Chem. Soc.* 129:4870–71
122. Warren MM, Kaucikas M, Fitzpatrick A, Champion PM, Sage JT, van Thor JJ. 2013. Ground-state proton transfer in the photoswitching reactions of the fluorescent protein Dronpa. *Nat. Commun.* 4:1461
123. Fron E, Sliwa M, Adam V, Michiels J, Rocha S, et al. 2014. Excited state dynamics of the photoconvertible fluorescent protein Kaede revealed by ultrafast spectroscopy. *Photochem. Photobiol. Sci.* 13:867–74
124. Krueger TD, Tang L, Zhu L, Breen IL, Wachter RM, Fang C. 2020. Dual illumination enhances transformation of an engineered green-to-red photoconvertible fluorescent protein. *Angew. Chem. Int. Ed.* 59:1644–52
125. Adam V, Lelimousin M, Boehme S, Desfonds G, Nienhaus K, et al. 2008. Structural characterization of IrisFP, an optical highlighter undergoing multiple photo-induced transformations. *PNAS* 105:18343–48
126. Duan C, Adam V, Byrdin M, Ridard J, Kieffer-Jaquinod S, et al. 2013. Structural evidence for a two-regime photobleaching mechanism in a reversibly switchable fluorescent protein. *J. Am. Chem. Soc.* 135:15841–50
127. Colletier J-P, Sliwa M, Gallat F-X, Sugahara M, Guillon V, et al. 2016. Serial femtosecond crystallography and ultrafast absorption spectroscopy of the photoswitchable fluorescent protein IrisFP. *J. Phys. Chem. Lett.* 7:882–87
128. Bourgeois D, Adam V. 2012. Reversible photoswitching in fluorescent proteins: a mechanistic view. *IUBMB Life* 64:482–91
129. Kim H, Grunkemeyer TJ, Modi C, Chen L, Fromme R, et al. 2013. Acid-base catalysis and crystal structures of a least evolved ancestral GFP-like protein undergoing green-to-red photoconversion. *Biochemistry* 52:8048–59
130. Arpin PC, Turner DB, McClure SD, Jumper CC, Mirkovic T, et al. 2015. Spectroscopic studies of cryptophyte light harvesting proteins: vibrations and coherent oscillations. *J. Phys. Chem. B* 119:10025–34
131. Hontani Y, Kloz M, Polívka T, Shukla MK, Sobotka R, Kennis JTM. 2018. Molecular origin of photoprotection in cyanobacteria probed by watermarked femtosecond stimulated Raman spectroscopy. *J. Phys. Chem. Lett.* 9:1788–92
132. Hontani Y, Inoue K, Kloz M, Kato Y, Kandori H, Kennis JTM. 2016. The photochemistry of sodium ion pump rhodopsin observed by watermarked femto- to submillisecond stimulated Raman spectroscopy. *Phys. Chem. Chem. Phys.* 18:24729–36
133. Pecourt JM, Peon J, Kohler B. 2001. DNA excited-state dynamics: ultrafast internal conversion and vibrational cooling in a series of nucleosides. *J. Am. Chem. Soc.* 123:10370–78
134. Baker LA, Horbury MD, Greenough SE, Coulter PM, Karsili TNV, et al. 2015. Probing the ultrafast energy dissipation mechanism of the sunscreen oxybenzone after UVA irradiation. *J. Phys. Chem. Lett.* 6:1363–68

135. Miller RJD. 1991. Vibrational energy relaxation and structural dynamics of heme proteins. *Annu. Rev. Phys. Chem.* 42:581–614
136. Zhu L, Sage JT, Champion PM. 1994. Observation of coherent reaction dynamics in heme proteins. *Science* 266:629–32
137. Mizutani Y, Kitagawa T. 1997. Direct observation of cooling of heme upon photodissociation of carbonmonoxy myoglobin. *Science* 278:443–46
138. Sagnella DE, Straub JE, Jackson TA, Lim M, Anfinrud PA. 1999. Vibrational population relaxation of carbon monoxide in the heme pocket of photolyzed carbonmonoxy myoglobin: comparison of time-resolved mid-IR absorbance experiments and molecular dynamics simulations. *PNAS* 96:14324–29
139. Kruglik SG, Lambry J-C, Martin J-L, Vos MH, Negrerie M. 2011. Sub-picosecond Raman spectrometer for time-resolved studies of structural dynamics in heme proteins. *J. Raman Spectrosc.* 42:265–75
140. Pontecorvo E, Ferrante C, Elles CG, Scopigno T. 2013. Spectrally tailored narrowband pulses for femtosecond stimulated Raman spectroscopy in the range 330–750 nm. *Opt. Express* 21:6866–72
141. Kuramochi H, Fujisawa T, Takeuchi S, Tahara T. 2017. Broadband stimulated Raman spectroscopy in the deep ultraviolet region. *Chem. Phys. Lett.* 683:543–46
142. Englman R, Jortner J. 1970. The energy gap law for radiationless transitions in large molecules. *Mol. Phys.* 18:145–64
143. Saar BG, Freudiger CW, Reichman J, Stanley CM, Holtom GR, Xie XS. 2010. Video-rate molecular imaging in vivo with stimulated Raman scattering. *Science* 330:1368–70
144. Opilik L, Schmid T, Zenobi R. 2013. Modern Raman imaging: vibrational spectroscopy on the micrometer and nanometer scales. *Annu. Rev. Anal. Chem.* 6:379–98
145. Wei L, Chen Z, Shi L, Long R, Anzalone AV, et al. 2017. Super-multiplex vibrational imaging. *Nature* 544:465–70
146. Ploetz E, Laimgruber S, Berner S, Zinth W, Gilch P. 2007. Femtosecond stimulated Raman microscopy. *Appl. Phys. B* 87:389–93
147. Min W, Freudiger CW, Lu S, Xie XS. 2011. Coherent nonlinear optical imaging: beyond fluorescence microscopy. *Annu. Rev. Phys. Chem.* 62:507–30
148. Ortega-Arroyo J, Kukura P. 2016. Non-fluorescent schemes for single-molecule detection, imaging and spectroscopy. *Nat. Photon.* 10:11–17
149. Tipping WJ, Lee M, Serrels A, Brunton VG, Hulme AN. 2016. Stimulated Raman scattering microscopy: an emerging tool for drug discovery. *Chem. Soc. Rev.* 45:2075–89
150. Fu D. 2017. Quantitative chemical imaging with stimulated Raman scattering microscopy. *Curr. Opin. Chem. Biol.* 39:24–31
151. Chen C, Baranov MS, Zhu L, Baleeva NS, Smirnov AY, et al. 2019. Designing redder and brighter fluorophores by synergistic tuning of ground and excited states. *Chem. Commun.* 55:2537–40
152. Wang L, Xie JM, Deniz AA, Schultz PG. 2003. Unnatural amino acid mutagenesis of green fluorescent protein. *J. Org. Chem.* 68:174–76
153. Peeler JC, Mehl RA. 2012. Site-specific incorporation of unnatural amino acids as probes for protein conformational changes. In *Unnatural Amino Acids: Methods and Protocols*, ed. L Pollegioni, S Servi, pp. 125–34. New York: Humana
154. Miller RJD. 2014. Femtosecond crystallography with ultrabright electrons and X-rays: capturing chemistry in action. *Science* 343:1108–16
155. Nogly P, Weinert T, James D, Carbajo S, Ozerov D, et al. 2018. Retinal isomerization in bacteriorhodopsin captured by a femtosecond X-ray laser. *Science* 361:eaat0094